Metal Ion-Induced Self-Assembly of Functionalized 2,6-Oligopyridines. 3. Metal–Metal Interaction and Redox State-Induced Transformations in Double-Stranded Helicates Derived from Functionalized Quinquepyridine and Sexipyridine[1]

Kevin T. Potts,*,† Majid Keshavarz-K,† Fook S. Tham,† Héctor D. Abruña,*,‡ and Claudia Arana‡

Departments of Chemistry, Rensselaer Polytechnic Institute, Troy, New York 12180, and Cornell University, Ithaca, New York 14853

Received April 15, 1993

4′,4‴-Bis(alkylthio)-2,2′:6′,2″:6″,2‴:6‴,2⁗-quinquepyridine yielded at ambient temperature double-stranded, bimetallic helical complexes of composition $[L_2M_2OAc]^{3+}$ with Fe(II), Co(II), Ni(II), and Zn(II); with Pd(II) the complex composition was $[L_2M_2]^{4+}$. X-ray data for the Ni(II) complex showed the two ligand strands intertwined about each other and around the two metal ions in a double helical fashion, the metal ions having distorted octahedral geometry and different chemical environments (N_6 and N_4O_2) with a supplementary bidentate acetate ligand completing the coordination shell of one of the Ni(II) ions. 4′,4⁗-Bis(alkylthio)-2,2′:6′,2″:6″,2‴:6‴,2⁗:6⁗,2⁗′-sexipyridines yielded analogous but symmetrical double-stranded bimetallic complexes with Fe(II), Co(II), Ni(II), and Cu(II), the X-ray structure of the Cu(II) complex showing the metals' distorted octahedral geometry and identical chemical environments (N_6, N_6). The S-*n*-propyl substituents in diamagnetic complexes were used as an ^1H NMR probe for demonstrating helical chirality and establishing the solution integrity of the complexes in different solvents. Electrochemical techniques and measured values of $\Delta E^{\circ\prime}$ (difference in formal potential) were used to show that metal–metal interaction occurred in the symmetrical homobimetallic systems; e.g., in the Co(II) complex the $\Delta E^{\circ\prime}$ for the Co centers' oxidation [i.e., Co(II/III)] and reduction [i.e., Co(II/I)] were 390 and 130 mV, respectively. The sexipyridine ligand also gave a trimetallic Cu(I) helical complex $[L_2Cu^I_3]$ with the Cu centers having tetrahedral geometry and the same chemical environments (N_4, N_4, N_4). Redox-induced transformations between trimetallic Cu(I) and bimetallic Cu(II) complexes were demonstrated chemically and verified spectroelectrochemically.

Introduction

The design and synthesis of metal complexes capable of metal–metal interaction[2] present many challenges and continue to be an area of great interest. In this publication we describe results obtained with transition metal complexes of the ligands 4′,4‴-bis(alkylthio)-2,2′:6′,2″:6″,2‴:6‴,2⁗-quinquepyridine (mt- or pt-qnpy; mt = methylthio, pt = *n*-propylthio) and 4′,4⁗-bis-(alkylthio)-2,2′:6′,2″:6″,2‴:6‴,2⁗:6⁗,2⁗′-sexipyridine (mt- or pt-sexpy). The mt- or pt-qnpy is potentially a pentadentate ligand. The ligating centers may collectively bind to one metal, as in the formation of heptacoordinate Co(II) helical complexes,[3a] which were also obtained from unsubstituted and 4-chlorophenyl-substituted quinquepyridines,[3b] and Ag(I) complexes, formed from unsubstituted quinquepyridine.[4] In a previous publication we described[5a] the synthesis and redox properties of double-stranded helical complexes of mt- and pt-qnpy containing Cu(II) and a mixed-valence Cu(II)/Cu(I) species as well as a trimetallic Cu(I) complex derived from the mt-qnpy ligand. All showed rich redox properties, especially the mixed-valence helicate in which significant metal–metal interaction was observed. The behavior of these mt- and pt-qnpy ligands with other transition metals is also of interest, and our results are reported in this publication. Establishing the integrity and the symmetry of these complexes in solution is of great importance. The number of nonequivalent aromatic protons and the spin system of the *S*-*n*-propyl substituents' protons in the ligands and in the complexes have provided unique information in this regard.

The hexadentate character of alkylthio-sexpy manifests itself in three principle ways: The ligating centers may collectively bind to one metal,[6] they may behave as three bipy units, or they may behave as two terpy units, as was found[7] recently in the Cd(II) complex of the unsubstituted ligand. Our results utilizing the last two coordination behaviors in a variety of metal ion-induced self-assembly processes, and the redox-induced transformations of the resultant double-stranded helical complexes, are described below. The redox properties of the Co(II) and Fe(II) complexes establish that significant metal–metal interaction occurs in these complexes.

† Rensselaer Polytechnic Institute.
‡ Cornell University.

(1) (a) Abstracted in part from the Ph.D. dissertations of M.K. (RPI, 1992) and C.A. (Cornell, 1992).
(2) (a) Gagne, R. R.; Spiro, C. L. *J. Am. Chem. Soc.* **1980**, *102*, 1443. (b) Powers, M. J.; Meyer, T. J. *J. Am. Chem. Soc.* **1980**, *102*, 1389. (c) Creutz, C.; Taube, H. J. *J. Am. Chem. Soc.* **1969**, *91*, 3988. Creutz, C.; Taube, H. J. *J. Am. Chem. Soc.* **1973**, *95*, 1086. (d) Campagna, S.; Denti, G.; Serroni, S.; Ciano, M.; Balzani, V. *Inorg. Chem.* **1991**, *30*, 3728. (e) Balzani, V.; Scandola, F. *Supramolecular Photochemistry*; Horwood: Chichester, U.K., 1991. Steel, P. J. *Coord. Chem. Rev.* **1990**, *106*, 227.
(3) (a) Gheysen, K. A.; Potts, K. T.; Hurrell, H. C.; Abruña, H. D. *Inorg. Chem.* **1990**, *29*, 1589. (b) Constabae, E. C.; Walker, J. V.; Tocher, D. A.; Daniels, M. A. M. *J. Chem. Soc., Chem. Commun.* **1992**, 768.
(4) Constable, E. C.; Drew, M. G. B.; Forsyth, G.; Ward, M. D. *J. Chem. Soc., Chem. Commun.* **1988**, 1450.
(5) (a) Potts, K. T.; Keshavarz-K. M.; Tham, F. S.; Abruña, H. D.; Arana, C. *Inorg. Chem.*, preceding paper in this issue. (b) Potts, K. T. *Bull. Soc. Chim. Belg.* **1990**, *99*, 741. For related helical complexes see: (c) Pfeil, A.; Lehn, J.-M. *J. Chem. Soc., Chem. Commun.* **1992**, 838. Lehn, J.-M. *Angew. Chem., Int. Ed. Engl.* **1990**, *29*, 1304. (d) Rüttimann, S.; Piguet, C.; Bernardinelli, G.; Bocquet, B.; Williams, A. F. *J. Am. Chem. Soc.* **1992**, *114*, 4230. Piguet, C.; Bernardinelli, G.; Bocquet, B.; Quattropani, A.; Williams, A. F. *J. Am. Chem. Soc.* **1992**, *114*, 7440. Also see refs 7 and 10.
(6) Constable, E. C.; Chotalia, R.; Tocher, D. A. *J. Chem. Soc., Chem. Commun.* **1992**, 771.
(7) (a) Constable, E. C.; Ward, M. D.; Tocher, D. A. *J. Am. Chem. Soc.* **1990**, *112*, 1256. (b) Constable, E. C.; Ward, M. D.; Tocher, D. A. *J. Chem. Soc., Dalton Trans.* **1991**, 1675. (c) Constable, E. C. *Tetrahedron* **1992**, *48*, 10013.
(8) Potts, K. T.; Gheysen Raiford, K. A.; Keshavarz-K. M. *J. Am. Chem. Soc.* **1993**, *115*, 2793.
(9) (a) Jennings, W. B. *Chem. Rev.* **1975**, *75*, 307. (b) Gunther, H. *NMR Spectroscopy*; John Wiley & Sons: New York, 1980; Chapter VI. (c) Reference 5c. (d) Youinou, M. T.; Ziessel, R.; Lehn, J.-M. *Inorg. Chem.* **1991**, *30*, 2144.

0020-1669/93/1332-4436$04.00/0

Experimental Section

Ligand synthesis was as described earlier,[8] and electrochemical and spectroscopic characterizations were performed under the conditions and using the same instrumentation as reported in the previous publication.[5a]

General Procedures for the Preparation of $[M_2L_2OAc][PF_6]_3$ [M = Fe(II), Co(II), Ni(II), Zn(II)]. Synthesis of $[Ni^{II}_2(mt\text{-}qnpy)_2OAc][PF_6]_3$ (2c). 4′,4‴-Bis(methylthio)-2,2′:6′,2″:6″,2‴:6‴,2⁗-quinquepyridine (mt-qnpy) (**1a**) (200 mg, 4.17×10^{-4} mol) was added to a solution of $Ni(OAc)_2 \cdot 4H_2O$ (103 mg, 4.17×10^{-4} mol) in methanol (20 mL). After being stirred for 3 h at room temperature, the pale-green solution was treated with a saturated, methanolic solution of ammonium hexafluorophosphate (200 mg). The resultant pale-green salt was filtered out and washed with methanol. Recrystallization from nitromethane:diethyl ether produced green microneedles: 325 mg (100%); mp > 300 °C (Table I).

Synthesis of $[Pd^{II}(pt\text{-}qnpy)][PF_6]_4$ (2e). The ligand **1b** (100 mg, 1.86×10^{-4} mol) and $Pd(OAc)_2$ (42 mg, 1.86×10^{-4} mol) in methanol (15 mL) were reacted together as above. The resultant orange salt crystallized from acetonitrile:diethyl ether as orange needles: 160 mg (92%); mp 280 °C with prior sublimation starting at 235 °C (Table I); ^1H NMR data (500 MHz, CD_3NO_2) δ 9.39 (bd, 2H), 8.41 (m, 2H), 8.39 (m, 2H), 8.25 (m, 4H), 8.12 (m, 4H), 7.98 (d, 2H), 7.96 (d, 2H), 7.91 (d, 2H), 7.75 (m, 2H), 7.37 (m, 2H), 7.22 (d, 2H), 7.20 (m, 2H), 6.75 (bd, 2H), 3.47 (m, 4H), 3.04 (m, 4H), 1.99 (m, 4H and CHD_2CN), 1.83 (m, 4H), 1.24 (t, 6H), 1.15 (t, 6H).

General Procedure for the Preparation of $[M(mt\text{-}sexpy)][PF_6]_4$ [M = Cu(II), Ni(II), Co(II)]. Synthesis of $[Cu^{II}(mt\text{-}sexpy)][PF_6]_4$ (5a). 4′,4⁗-Bis(methylthio)-2,2′:6′,2″:6″,2‴:6‴,2⁗:6⁗,2⁗′-sexipyridine (mt-sexpy) (**4a**) (100 mg, 1.79×10^{-4} mol) was added to a solution of $Cu(OAc)_2 \cdot H_2O$ (36 mg, 1.8×10^{-4} mol) in methanol (10 mL). After being stirred for 4 h at room temperature, the resultant green solution was treated with a saturated, methanolic solution of ammonium hexafluorophosphate (150 mg). A green salt precipitated, which was collected, washed with methanol, and then recrystallized from CH_3CN:diethyl ether forming green prisms: 163 mg (100%); mp > 300 °C (Table II).

Preparation of $[Fe^{II}(pt\text{-}sexpy)][ClO_4]_4$ (5c). The ligand **4b** (100 mg, 1.6×10^{-4} mol) was added to a solution of ferrous perchlorate (58 mg, 1.6×10^{-4} mol) in acetonitrile (15 mL). An immediate solution color change to dark-red occurred, and after stirring of the reaction mixture for 2 h at room temperature, the complex was precipitated by the addition of diethyl ether (15 mL). The resultant red product was collected and washed with methanol followed by diethyl ether: 125 mg (90%). Recrystallization from acetonitrile:diethyl ether produced red-black needles: 105 mg, 76%; mp 270 °C (severe decomposition) (Table II). *Caution! The thermal decomposition indicates that this perchlorate should be handled with care.*

Preparation of $[Cu^{I}_3(pt\text{-}sexpy)_2][PF_6]_3$ (6). The ligand **4b** (100 mg, 1.6×10^{-4} mol) was added to a solution of $[Cu^{I}(CH_3CN)_4][PF_6]$ (91 mg, 2.45×10^{-4} mol) under a N_2 atmosphere in oxygen-free acetonitrile (10 mL). The initially colorless solution immediately changed to black, and after stirring of the reaction mixture for 2 h, the slow addition of diethyl ether (20 mL) caused the complex to separate. The resultant black prisms were collected, washed with methanol followed by diethyl ether, and then dried in a vacuum desiccator: 115 mg (78%); mp 310–312 °C (Table II). The analogous complex formed from ligand **4a** gave similar results.

X-ray Structural Determinations. Crystal selection and mounting were done in the cold room (2 °C) to avoid loss of solvent of crystallization which caused marked deterioration of the crystal. After dipping of the selected crystal into epoxy resin, it was attached onto a glass fiber before the epoxy hardened, and after being set aside for 1 h, the crystal was mounted on a goniometer head. Siemens standard procedures and programs were used for all operations.

Crystal Data for 2c: $C_{56}H_{45}N_{10}Ni_2O_2S_4(PF_6)_3 \cdot 6.64H_2O$, orthorhombic dark-green prism of 0.24 × 0.25 × 0.28 mm, M = 1690.3, space group *Pnna* (No. 52), a = 16.896(2) Å, b = 25.715(3) Å, c = 16.300(3) Å, $\alpha = \beta = \gamma = 90°$, V = 7082(2) Å^3, Z = 4, D_c = 1.585 Mg m^{-3}. Data were collected at room temperature (21 °C) using a Siemens R3m diffractometer with Cu Kα radiation (graphite monochromator; λ = 1.541 78 Å) in a Wyckoff scan mode ($\omega = 1.20° + [2\theta(K\alpha_1) - 2\theta(K\alpha_2)]$; 2θ range = 3–115°). The reflections were measured with a variable scan speed (5.00–29.30°/min) and an ω scan range of 1.20°, four check reflections being measured for every 60 reflections in a total of 5385 reflections collected, of which 2999 reflections were uniquely observed ($F > 4.0\sigma(F)$) Lorentz, polarization, and semi-empirical absorption corrections were applied [μ(Cu) = 3.36 mm^{-1}]. Siemens programs, SHELXTL PLUS (release 4.21/V), were used for phase determinations and structure refinements. Systematically absent reflections and distribution of intensities ($E^2 - 1 = 0.991$) indicated a centrosymmetric space group, *Pnna* (No. 52), and data were refined using this space group. The positions of the Ni atoms were identified in a Patterson vector map, and direct methods of phase determination led to an electron-density map from which the non-hydrogen atoms were identified, except the oxygen atoms of waters of crystallization. The Ni cation complex was located along the unique 2-fold rotation axis parallel to the a-axis. One phosphorous atom of the three hexafluorophosphate anions is located on an inversion center, and two carbon atoms of the acetate group are also located along the unique 2-fold axis on which the Ni atoms are located. Subsequent isotropic refinement led to the identification of four molecules of water where two of the sites were partially (64% and 68%) occupied. The oxygen atoms of these four water molecules have relatively high thermal motions. Atomic coordinates and isotropic and anisotropic temperature factors of all non-hydrogen atoms were refined by means of a full-matrix least-squares procedure. Because the acetate carbons are located along the unique 2-fold rotation axis, the methyl hydrogens of the acetate group are inherently present in two conformations, with 50% site occupancy for each conformation. All hydrogen atoms were included in calculated positions riding on the atoms to which they were attached and with fixed isotropic temperature factors. The refinement converged at R = 6.94% and R_w = 10.86%. The background in the electron density map was 0.36 e/Å^3.

Crystal Data for 5a: $C_{64}H_{48}Cu_2N_{12}S_4PF_{64} \cdot 3.8CH_3CN$, monoclinic green prism of 0.10 × 0.44 × 0.48 mm, M = 1976.9, space group $P2_1/c$ (No. 14), a = 14.515(3) Å, b = 28.426(7) Å, c = 20.370(4) Å, β = 90.45(2)°, V = 8404(3) Å^3, Z = 4, D_c = 1.562 Mg m^{-3}. Using the procedures described for **2c** [with the following parameters: ω scan range = 1.20°; 2θ = 3–116°; variable scan speed = 5.00–29.30°/min; μ(Cu) = 3.21 mm^{-1}; 12511 reflections collected, 6456 unique reflections ($F > 4.0\sigma(F)$], systematically absent reflections and distribution of intensities ($E^2 - 1 = 1.119$) indicated a centrosymmetric space group, $P2_1/c$ (No. 14), and the data were refined using this space group. The positions of the two Cu atoms were identified in a Patterson vector map. Direct methods of phase determination led to an electron-density map from which the non-hydrogen atoms were identified, except the four molecules of acetonitrile of crystallization which were identified on subsequent isotropic refinement. One of these molecules was partially occupied (81%). Atomic coordinates and isotropic and anisotropic temperature factors of all non-hydrogen atoms were refined by means of a blocked full-matrix least-squares procedure. All hydrogen atoms were included in the refinement in calculated positions riding on the atoms to which they were attached and with fixed isotropic temperature factors. The refinement converged at R = 6.93% and R_w = 10.70%. The background in the electron-density map was 0.73 e/Å^3.

Results and Discussion

Functionalized Quinquepyridines: Bimetallic Helicates with Octahedral Coordination Geometry. The alkylthio-substituted quinquepyridines (mt- or pt-qnpy) are appreciably soluble in most organic solvents and are well suited for studying metal ion-induced self-assembly processes at ambient temperature. Our work involving the formation of double-stranded bimetallic helicates is shown in Scheme I. Reaction of ligand **1a** with $Co(OAc)_2 \cdot 4H_2O$ in methanol followed by counterion exchange gave the golden, high-spin hexafluorophosphate salt $[Co^{II}_2(mt\text{-}qnpy)_2OAc][PF_6]_3$ (**2b**), which was also prepared in a stepwise fashion by rearrangement of monomeric **3** with a large excess of NH_4OAc in methanol. The molecular formula and dimeric nature of **2b**, as well as other complexes (Tables I and II) described in this publication, were established from combustion analytical data and FAB mass spectral data, and for **2b**, the latter data are shown in Table IV and Figure 7. Electrochemical data (Figures 8 and 11; Table VI) show that the dimeric structure **2b** was retained in solution (CH_3CN). Additional evidence comes from the NMR spectrum of **2b** discussed later, which is shown in Figure 5 together with that of the monomeric complex **3**.

Reaction of the ligand **1a** with $M(OAc)_2 \cdot xH_2O$ [M = Fe(II), Ni(II), and Zn(II)] in methanol at ambient temperature also yielded double-stranded bimetallic helical complexes, isolated as their hexafluorophosphate salts (Table I). The X-ray structure of the Ni(II) complex (Figure 1) shows the complex to have a

Table I. Bimetallic, Double-Stranded Helicates[a] **2** Derived from the Quinquepyridine Ligand[b] **1**

complex no.	complex compsn	color, cryst habit: solvent[c]	molecular formula	anal. data calcd (found) % C	% H	% N	mass spectral data,[d] m/z (% rel intensity)	UV/vis spectral data (CH_3CN), λ_{max}, nm (ϵ, (cm M)$^{-1}$)	magnetic moment, μ_B (per metal)
2a	$[Fe^{II}_2L_2CH_3COO][PF_6]_3$	yellow microneedles: B	$C_{56}H_{45}F_{18}Fe_2N_{10}O_2P_3S_4 \cdot CH_3NO_2$	43.64 (43.58)	2.78 (2.97)	9.48 (9.74)	1393.3 (11) $[Fe_2L_2OAcPF_6F]$, 534.8 (100) $[Fe(L)^+]$	214 (5.79×10^4), 232 (5.51×10^4), 298 (4.41×10^4)	8.9 (4.5)
2b	$[Co^{II}_2L_2CH_3COO][PF_6]_3$	gold needles: C	$C_{56}H_{45}Co_2F_{18}N_{10}O_2P_3S_4 \cdot H_2O$	42.33 (42.00)	2.99 (2.89)	8.81 (8.73)	1424.9 (18) $[M^+ - PF_6]$, 1280.6 (8) $[M^+ - 2PF_6]$, 1221.4 (5) $[M^+ - 2PF_6 - (CH_3COO)]$, 538.3 $[Co(L)^+]$	202 (1.23×10^5), 250 (sh), 294 (8.97×10^4), 580 (51)	10.2 (5.1)
2c	$[Ni^{II}_2L_2CH_3COO][PF_6]_3$	green needles: B	$C_{56}H_{45}F_{18}N_{10}Ni_2O_2P_3S_4 \cdot H_2O$	42.34 (42.12)	2.89 (2.83)	8.81 (8.70)	1366.5(2) $[M^+ - PF_6 - (CH_3COO)]$, 1221.5 (2) $[M^+ - 2PF_6 - (CH_3COO)]$, 537.3 $[Ni(L)^+]$	198 (9.75×10^5), 250 (5.41×10^5), 298 (6.34×10^5)	7.1 (3.5)
2d	$[Zn^{II}_2L_2CH_3COO][PF_6]_3$	colorless prisms: D	$C_{56}H_{45}F_{18}N_{10}O_2P_3S_4Zn_2 \cdot H_2O \cdot C_4H_8O_2$	42.64 (42.77)	3.27 (3.02)	8.28 (8.37)	1492 (1) $[M^+ - PF_6]$,[e] 1347 (1) $[M^+ - 2PF_6]$,[e] 1202 (1) $[M^+ - 3PF_6]$[e]	208 (8.77×10^4), 242 (4.66×10^4), 292 (7.04×10^4)	diamagnetic
2e	$[Pd^{III}L]_2[PF_6]_4$	orange needles: A	$C_{62}H_{58}F_{24}N_{10}P_4Pd_2S_4 \cdot H_2O$	39.56 (39.40)	3.21 (3.24)	7.44 (7.30)	1429 (5) $[M^+ - 3PF_6]$, 1283 (4) $[M^+ - 4PF_6]$, 747 (3) $[LPd_2]$,	196 (1.41×10^5), 210 (1.40×10^5), 240 (9.82×10^4), 282 (9.35×10^4), 311, 346, 377 (sh)	diamagnetic

[a] All isolated as hexafluorophosphate salts in practically quantitative yield and had mp > 300 °C except for **2e**, mp 280 °C with sublimation starting at 235 °C. [b] All prepared from **1a** except **2e** where **1b** was used. [c] Crystallization solvents A = CH_3CN/Et_2O, B = CH_3NO_2/Et_2O, C = acetone/methanol, D = CH_3CN/dioxane. [d] FAB technique using 3-nitrobenzyl alcohol as matrix except for [e] where CF_3COOH was used, resulting in substitution of the CH_3COO group in the resultant ion.

Table II. Bi- and Trimetallic, Double-Stranded Helicates[a] Derived from Ligand[b] **4**

complex no.	complex composn	color, cryst habit	molecular formula	anal. data calcd (found) % C	% H	% N	mass spectral data, m/z (% rel intensity)	UV/vis spectral data (CH_3CN), λ_{max}, nm (ϵ, (cm M)$^{-1}$)	magnetic moment μ_B (per metal)
5a	$[Cu^{II}_2L_2][PF_6]_4$	green prisms	$C_{64}H_{48}Cu_2F_{24}N_{12}P_4S_4 \cdot 3H_2O$	41.01 (41.04)	2.90 (2.71)	8.96 (8.61)	1676.2 (2) $[M^+ - PF_6]$, 1530.7 (6) $[M^+ - 2PF_6]$, 1395.3 (7) $[M^+ - 3PF_6]$, 1240.2 (2) $[M^+ - 4PF_6]$, 620 (25) $[Cu(L)^+]$	222 (3.49×10^4), 294 (6.67×10^4), 330 (6.6×10^4)	5.7 (2.4)
5b	$[Ni^{II}_2L_2][PF_6]_4$	green prisms	$C_{64}H_{48}F_{24}N_{12}Ni_2P_4S_4 \cdot H_2O$	42.04 (42.07)	2.75 (2.49)	9.19 (9.44)	1663.2 (19) $[M^+ - PF_6]$, 1519.2 (12) $[M^+ - 2PF_6]$, 1374.1 (2) $[M^+ - 3PF_6]$, 615 (25) $[Ni(L)^+]$	198 (1.60×10^5), 298 (8.13), 321, 336, 350 (sh), 557 (44)	7.4 (3.7)
5c	$[Fe^{II}_2L_2][ClO_4]_4$	red-black needles	$C_{72}H_{64}Cl_4Fe_2N_{12}O_{16}S_4$	49.84 (49.54)	3.72 (3.67)	9.68 (9.61)	1635.1 (8) $[M^+ - ClO_4]$, 1536.4 (25) $[M^+ - 2ClO_4]$, 1435.2 (22) $[M^+ - 3ClO_4]$, 1336.1 (8) $[M^+ - 4ClO_4]$	198 (1.06×10^5), 208 (1.09×10^5), 290 (7.22×10^4), 340 (6.68×10^4), 508 (1.74×10^5)	10.5 (5.2)
5d	$[Co^{II}_2L_2][PF_6]_4$	greenish-gold needles	$C_{64}H_{48}Co_2F_{24}N_{12}S_4P_4 \cdot 2H_2O$	41.62 (41.62)	2.87 (2.69)	9.10 (9.08)	1664.2 (15) $[M^+ - PF_6]$, 1519.9 (13) $[M^+ - 2PF_6]$, 1374.7 (5) $[M^+ - 3PF_6]$, 1229.9 (7) $[M^+ - 4PF_6]$, 615.9 (25) $[Co(L)]^+$	200 (2.07×10^5), 294 (8.0×10^4), 310 (7.73×10^4), 350 (sh)	9.7 (4.8)
6	$[Cu^{I}_3L_2][PF_6]_3$	black needles	$C_{72}H_{64}Cu_3F_{18}N_{12}P_3S_4 \cdot 2H_2O$	45.83 (45.69)	3.63 (3.38)	8.90 (8.76)	1706.4 (55) $[M^+ - PF_6]$, 1560.7 (45) $[M^+ - 2PF_6]$, 1416.0 (12) $[M^+ - 3PF_6]$,	206 (2.25×10^4), 223 (1.92×10^4), 292 (1.84×10^4), 434 (2.41×10^4, 570 (1.79×10^5)	diamagnetic

[a] Obtained in >90% yield as hexafluorophosphate salts except **5c**, mp > 300 °C, and **5c**, mp 270 °C (severe decomposition); all crystallized from CH_3CN/Et_2O. [b] All prepared from ligand **4a** except **5c** and **6**, where **4b** was used.

Scheme I

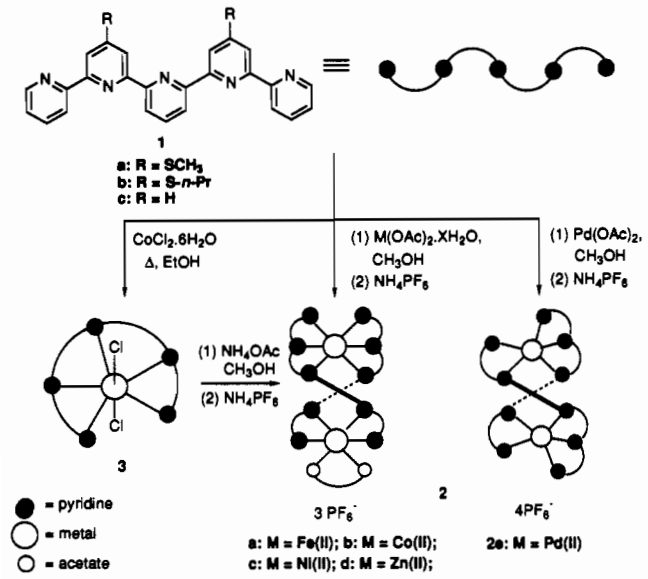

Scheme II

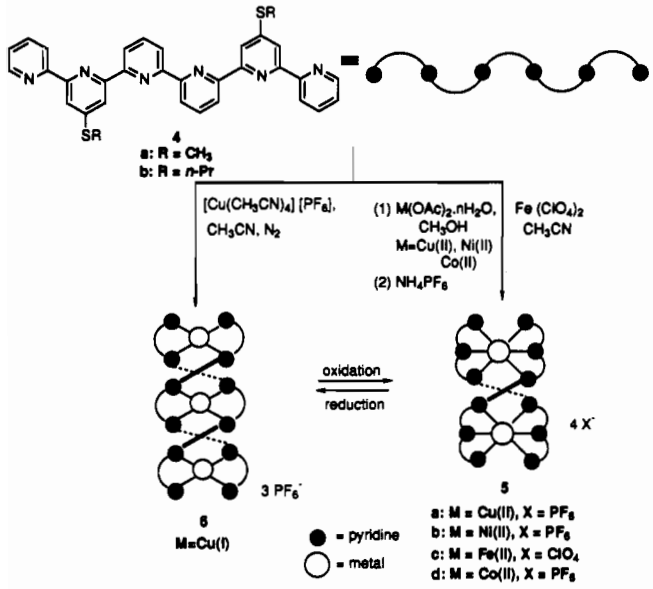

distorted octahedral environment around each metal (N_6, N_4O_2), the result of each ligand strand being intertwined about each other and around the two metals.

The ligand **1b** and $Pd(OAc)_2$ in methanol at ambient temperature resulted in the corresponding double-stranded helical complex **2e** (Table I) of composition $[LM]_2[PF_6]_4$. Formation of this asymmetrical complex containing pentacoordinated palladium requires the quinquepyridine ligand to behave as a bipy and as a terpy segment, and this coordination pattern was recently shown[10b] by the X-ray structure of the complex obtained from unsubstituted quinquepyridine.

Functionalized Sexipyridines: Bi- and Trimetallic Helicates with Octahedral and Tetrahedral Coordination Geometry. Sexipyridine is potentially a hexadentate ligand which may act as two terpyridine or three bipyridine subunits, forming bimetallic or trimetallic complexes, respectively, as shown in Scheme II. The ligand **4** with M(II) ions [M(II) = Fe(II), Co(II), Ni(II), and Cu(II)] yielded symmetrical double-stranded helical complexes **5**, all of which contain two metal ions in identical chemical environments (N_6, N_6) and which are described in Table II.

(10) (a) Constable, E. C.; Elder, S. M.; Raithby, P. R.; Ward, M. D. *Polyhedron* **1991**, 1395. (b) Constable, E. C.; Elder, S. M.; Healy, J.; Ward, M. D.; Tocher, D. A. *J. Am. Chem. Soc.* **1990**, *112*, 4590.

The molecular formulas of these complexes were readily established as above, and their helical nature was verified, in the case of the Cu(II) complex **5a**, by a X-ray structural determination (Figure 2). Both Cu ions had distorted octahedral geometries, and the two ligands were arranged in a double-stranded helical fashion about each other and the two Cu(II) ions. In the formation of the Fe(II) complex **5c**, $Fe(OAc)_2$ under the same reaction conditions as above did not result in a characterizable product. An alternative procedure using $Fe^{II}(ClO_4)_2 \cdot 6H_2O$ in acetonitrile solution (room temperature) was successful, and the complex was isolated as red-black needles (Table II). It is surprising that this iron complex is of high spin, unlike the bis(terpy)iron(II) complex, which is low spin. This difference could be the result of strain imposed on the octahedral environment of the iron cations in the double-stranded helical structure.

The ligand **4b** and $[Cu^{I}(CH_3CN)_4][PF_6]$ in oxygen-free acetonitrile (N_2 atmosphere) resulted in the trimetallic complex **6** (Table II), obtained as black needles. Its molecular formula was established by a combination of FAB mass spectral data and combustion analytical data. Reduction of the bimetallic Cu(II) complex **5a** with hydrazine hydrate in acetonitrile solution also gave the trimetallic complex **6**. The reverse process, conversion of **6** into **5a**, was achieved by air oxidation. This interesting redox-induced transformation was verified by spectroelectrochemical techniques as described below.

^{1}H NMR Characterization of Bi- and Trimetallic Helicates. A variety of data established the molecular formulas and the double-stranded helical nature of the complexes in the solid state. We have studied the structures of the complexes in solution using NMR, electrochemical, and electronic spectral techniques, and in our NMR studies the *S*-alkyl groups introduced into the pyridine 4-position during ligand synthesis for solubility and ultimate functional group manipulation behaved as convenient "built-in" NMR probes. In general, a substituent $-CH_2R$ group can serve as a ^{1}H NMR probe for determining the chirality of a molecule.[9a] The enantiotopic $-CH_2-$ group has an A_2 spin system in an achiral molecule (the ligand); when this $-CH_2-$ group is situated in a chiral environment, it becomes diastereotopic with an AB spin system[9b] (the complex). We have utilized this characteristic property to show the solution stability and helical chirality of several complexes containing *S*-*n*-propyl-substituted pyridine subunits in the ligand strand. One should note that this type of geminal coupling ($\Delta\delta$) can be affected by several factors. In general the couplings of these protons depend significantly on temperature and solvent as well as structure.[9a] In the case of the complex **2e** the second $-CH_2-$ group in the *S*-propyl group is, in principle, a diastereotopic center. However the magnitude of $\Delta\delta$ in complex **2e** is considerably depressed as the distance between the $-CH_2-$ groups and the asymmetric helical structure is appreciably greater than with the $-CH_2-$ group adjacent to the sulfur atom. $\Delta\delta$ of both $-CH_2-$ groups is solvent dependent, and sulfur's two lone pairs of electrons may also influence the solvent effect. The Pd(II) complex **2e** derived from the ligand **1b** illustrates this approach very effectively. Figures 3 and 4 show the ^{1}H NMR spectra in the aliphatic and aromatic regions, respectively, of the ligand and its complex. The lack of a C_2 rotating axis of symmetry perpendicular to the metal–metal axis results in two types of *n*-propyl groups with significantly different chemical shifts. Figure 3A shows the spectrum of the ligand **1b** with the $A_2M_2X_3$ spin system of the two equivalent *S*-*n*-propyl substituents. Figure 3B shows the spectrum of the complex **2e** in CD_3CN and the two non-equivalent propyl substituents. The *S*–CH_2- protons with an AB spin system are shown in expanded form in the inset.

Figure 4 clearly shows the difference in chemical shifts of the aromatic region of the ligand **1b** and the Pd(II) complex **2e**. The linear transoid ligand **1b** (Figure 4A) contains fifteen aromatic protons, yet only eight protons are nonequivalent due to the C_2

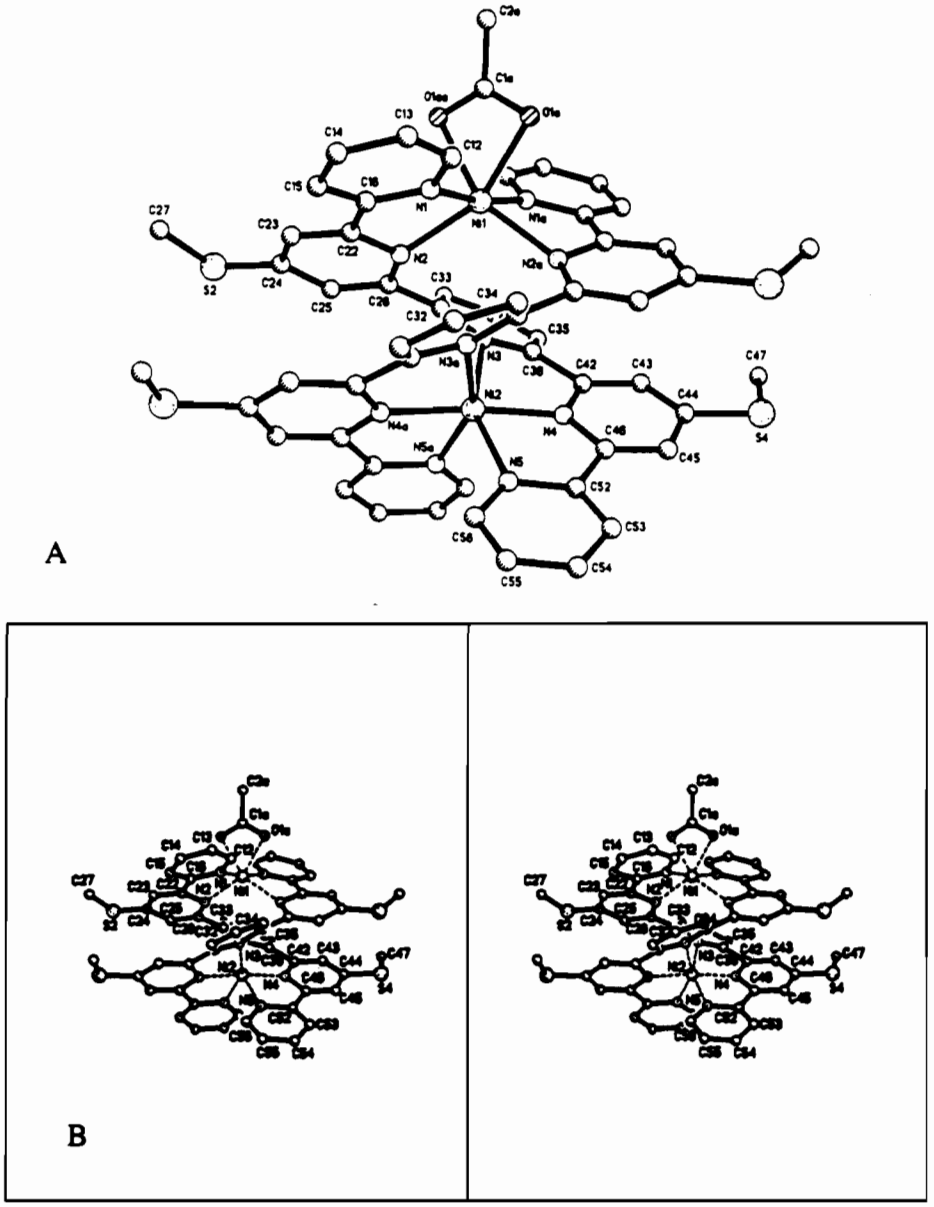

Figure 1. (A) X-ray structure of the right-handed (P) double-stranded helical Ni(II) complex **2c** derived from the ligand **1a** showing $\pi-\pi$ stacking between adjacent strands. (B) Stereotopic view of **2c** along the *b*-axis.

rotation symmetry axis bisecting the middle pyridine ring.[8] The spectrum of the double-stranded helical complex **2e** shows that all the fifteen protons are nonequivalent in each ligand strand (see Experimental Section). This nonequivalency is best demonstrated for the two terminal protons (H_6, $H_{6''''}$). In the ligand these protons are equivalent (δ 8.69) and, on complexation, one proton is shifted downfield (δ 9.27, CD_3CN) and the other proton is shifted upfield (δ 6.56, CD_3CN). These changes in chemical shifts are understandable in terms of the helical nature of the complex with the consequence that the ligand behaves as bipy and terpy segments (Scheme I). H_6 of each terpy segment is located in the shielding zone of the bipy segments in the other strand and undergoes an upfield shift. Conversely, the terminal proton in the bipy segment of the same strand is located in the deshielding zone and undergoes the observed downfield shift. It is interesting to compare these chemical shifts with those of bis(terpy) complexes, where only upfield shifts were observed,[11] and with tris(bipy) complexes, where only downfield shifts were observed.[12] The solvent dependency and the severe overlap of some of the chemical shifts in complex **2e** are shown in Figure 4B–D.

The high-spin paramagnetic Co(II) double-helical complex **2b** also lacks the C_2 rotation symmetry axis bisecting the middle pyridine ring, and as a consequence, all the aromatic protons are nonequivalent (Figure 5A). The high-spin paramagnetic Co(II) monomeric complex **3** possesses such a C_2 symmetry axis, and consequently, there are 8 nonequivalent aromatic protons (Figure 5B). A comparison of parts A and B of Figure 5 clearly demonstrates the solution integrity of the dimer **2b** in CH_3CN, in contrast to the Co(II) complexes derived[3b] from unsubstituted and 4-chlorophenyl-substituted quinquepyridines where no dimer was observed in solution.

The ^1H NMR spectrum of the trimetallic Cu(I) double-stranded complex **6** obtained from the sexipyridine ligand **4b** shows a very strong complexation effect although in this case there is an overall contraction of the aromatic region with an

(11) Elsberd, H.; Beattle, J. K. *Inorg. Chem.* **1972**, *34*, 771. Lytle, F. E.; Petrosky, M.; Carlson, R. *Anal. Chim. Acta* **1971**, *57*, 239.

(12) Birchall, J. D.; O'Donoghue, T. D.; Wood, J. R. *Inorg. Chim. Acta Lett.* **1979**, *37*, L461.

(13) Guadalupe, A. R.; Usifer, D. A.; Potts, K. T.; Hurrell, H. C.; Mogstad, A.-E.; Abruña, H. D. *J. Am. Chem. Soc.* **1988**, *110*, 3462.

(14) Potts, K. T.; Keshavarz-K. M.; Abruña, H. D.; Arana, C.; Trible, K.; Evans, D. Unpublished results.

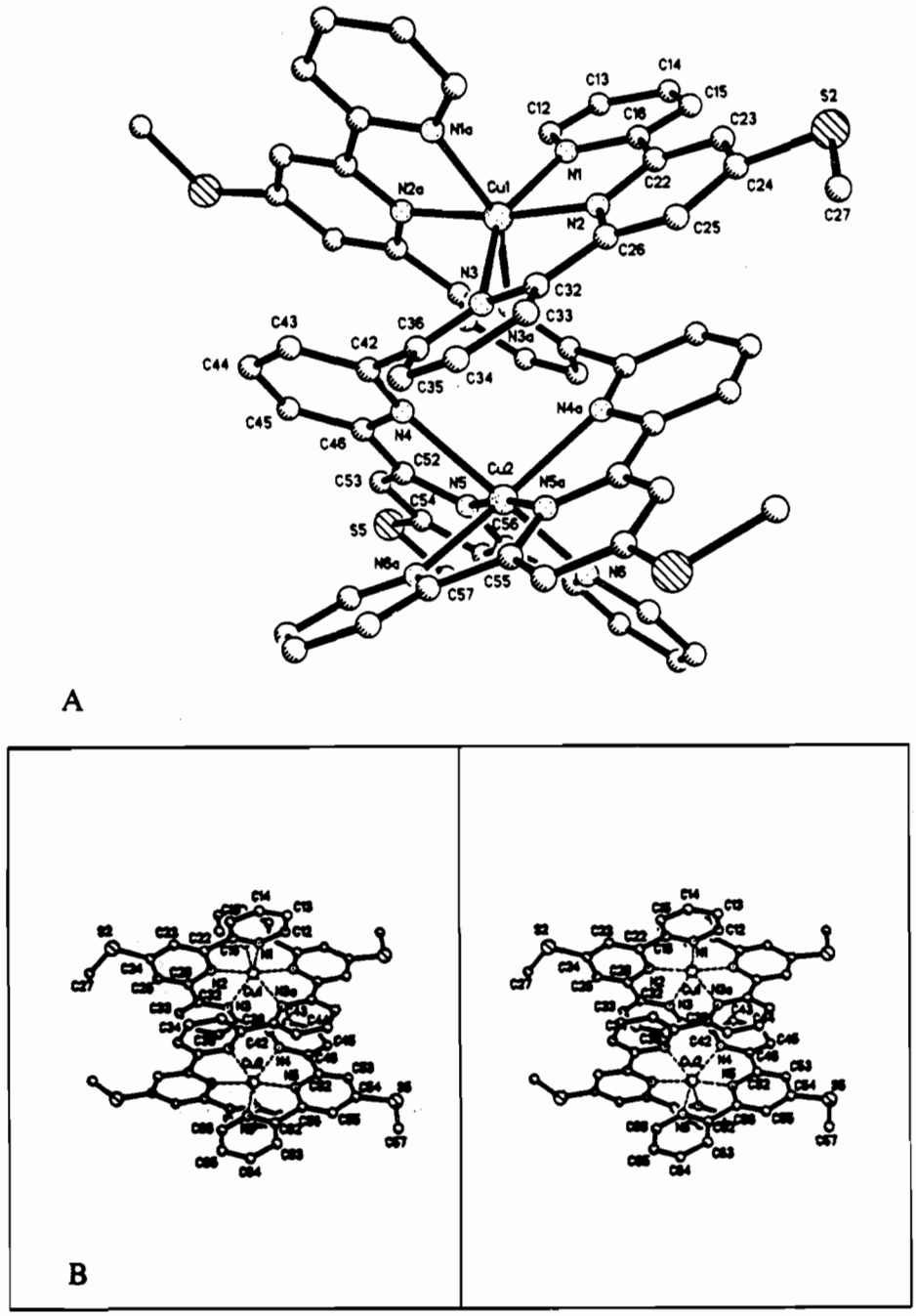

Figure 2. (A) X-ray structure of the right-handed (P) double-stranded helical Cu(II) complex **5a** derived from the ligand **4a** showing π–π stacking between adjacent strands. (B) Stereotopic view of **5a** along the *b*-axis.

overall upfield shift of the aromatic protons (Figure 6A,B). This effect is in contrast to that observed in the Pd(II) complex (Figure 4). The overall upfield shift of the aromatic protons is consistent with similar shifts observed in all Cu(I) double-stranded helical complexes derived from alkylthio-substituted oligopyridines from substituted terpyridines through octipyridine.[5a,15] The aromatic region (Figure 6B) of this trimetallic complex clearly shows the D_2 symmetry of the complex in solution. The 36 possible aromatic protons are reduced to 9 protons (Table III) as a result of both a C_2 rotation symmetry axis lying along the helical axis and a C_2 rotation axis bisecting the C–C interannular bond between the third and fourth pyridine rings of the sexipyridine ligand strand. The aliphatic region (Figure 6D) shows only one type of *S*-*n*-propyl group with a pronounced intramolecular diastereotopic effect.

(15) Potts, K. T.; Keshavarz-K. M.; Tham, F. S.; Abruña, H. D.; Arana, C. *Inorg. Chem.*, submitted for publication.

Mass Spectral Characterization of Bi- and Trimetallic Helicates. The FAB mass spectra of these bi- and trimetallic complexes are important in their characterization, and in addition to the data reported in Tables I and II, several comments are appropriate. Spectra of the bimetallic complexes derived from the mt-quinquepyridine ligand **1a** and the mt-sexipyridine ligand **4a** show similar fragmentation, and although the complexes themselves are multiply charged, the fragmentation resulting from the FAB experiment (3-nitrobenzyl alcohol matrix) usually resulted in singly-charged ions with an occasional doubly-charged ion. The observed ions were mainly the result of cleavages of the metal/ligand bonds with very little fragmentation of the ligands themselves. For example, the sexipyridine ligand **4a** showed one intense ion, m/z 557.2, corresponding to the [M + 1] ion, with very little further fragmentation occurring. The spectra of the complexes typically showed a series of clusters resulting from the sequential loss of the counterions, the most abundant ion

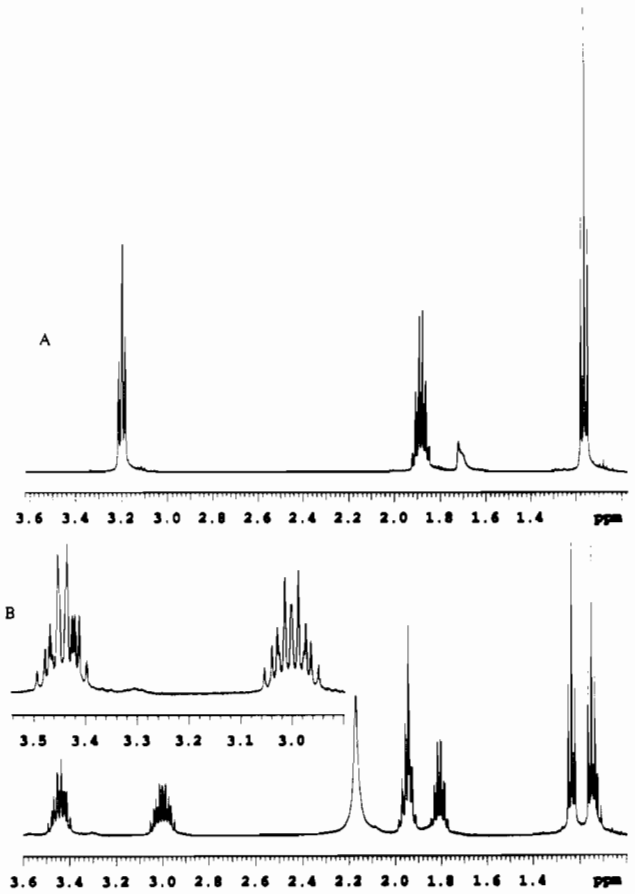

Figure 3. ^{1}H NMR spectra (aliphatic region) (500 MHz) of the double-stranded helical Pd(II) complex **2e** derived from the ligand **1b**: (A) Ligand **1b** in $CDCl_3$; (B) complex **2e** in CD_3CN. Inset: Expanded portion of S–CH_2– of **2e**.

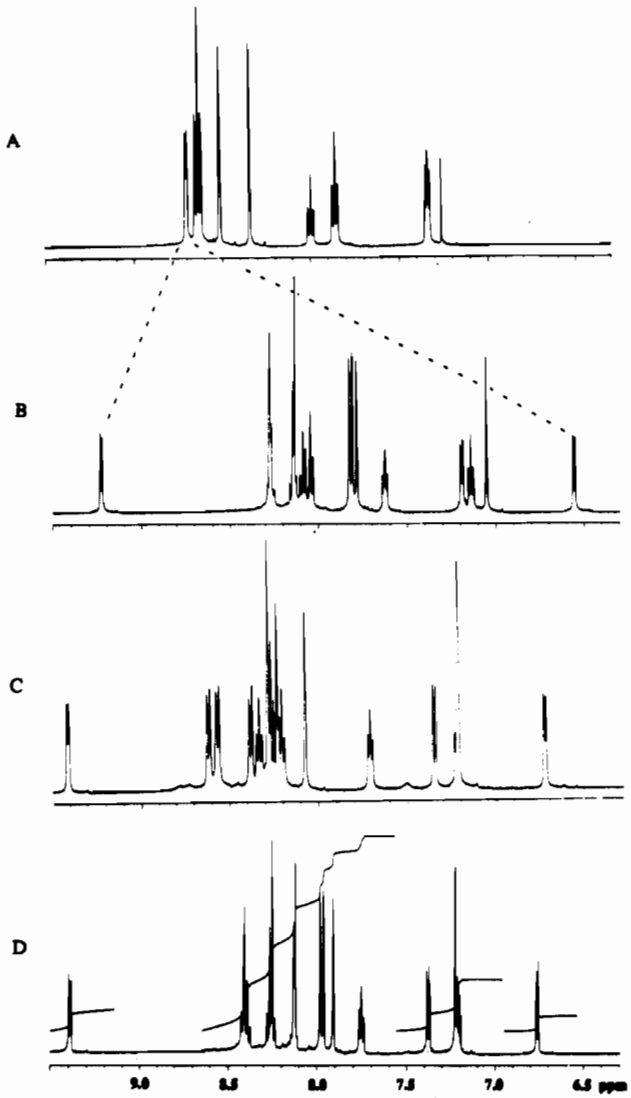

Figure 4. ^{1}H NMR spectra (aromatic region) (500 MHz) of (A) ligand **1b** in $CDCl_3$ and complex **2e** in (B) CD_3CN, (C) DMSO-d_6 and (D) CD_3NO_2.

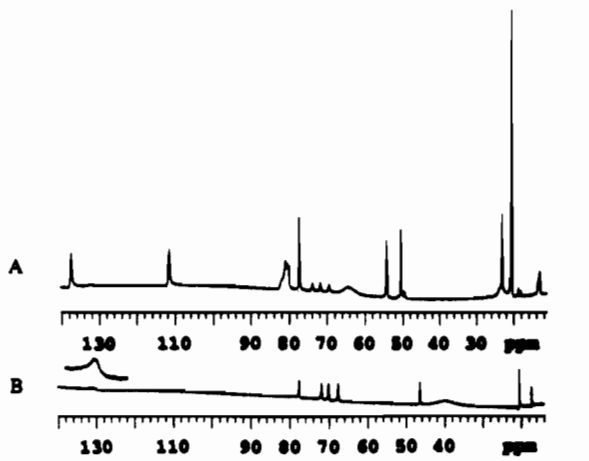

Figure 5. ^{1}H NMR spectra (aromatic region) (500 MHz) (paramagnetically shifted) of (A) the dimeric Co(II) complex **2b** in CD_3CN and (B) the monomeric Co(II) complex **3** in CD_3CN:D_2O (1:2).

corresponding to the loss of one or two $[PF_6]^-$ ions and, in the case of the mt-qnpy complexes, the loss of the weakly bonded acetate group. Within each cluster there were ions corresponding to the isotopic distributions and, in addition, an ion at 19 mass units higher than the most abundant cluster ion accountable for by a species containing an additional fluorine atom derived from a $[PF_6]^-$ counterion. An additional ion at 14 mass units lower than the most abundant cluster ion is consistent with the loss of a CH_2 group from the ligand's methylthio substituent. The complex $[Co^{II}_2(mt\text{-}qnpy)_2OAc][PF_6]^3$ (**2b**) serves to illustrate the fragmentation behavior of the acetate-containing complexes. Table IV lists the assignments for the most abundant ions in its mass spectrum. The ion at m/z 1385, attributed to $[Co^{II}_2(mt\text{-}qnpy)_2(PF_6)_2F]^+$ is consistent with the loss of the acetate group and the transfer of a fluoride ion from a $[PF_6]^-$ counterion to the singly charged complex with the accompanying loss of a neutral PF_5 species. This transfer of a fluoride ion does not require the loss of an acetate group, as evidenced by an intense ion at m/z 1425 attributed to the $[Co^{II}_2(mt\text{-}qnpy)_2OAc(PF_6)_2]^+$ ion (see Figure 7 below). A similar ion m/z 1459 corresponding to the $[Zn^{II}_2(mt\text{-}qnpy)_2OAc(PF_6)_2F]^+$ ion was observed in the analogous Zn(II) complex **2d**. Figure 7 shows the observed and calculated ion intensities based on isotopic distributions for the ion $[Co^{II}_2(mt\text{-}qnpy)_2OAc(PF_6)_2]^+$ and illustrates the use of the unique isotopic distribution pattern of each metal-containing ion in facilitating identification and serving as a fingerprint for that particular ion. In this instance it also provides compelling evidence for the dimetallic nature of the complex.

Electronic Spectra. The band maxima (λ_{max}) and molar absorptivities (ϵ) for these complexes are listed in Tables I and II. The absorption spectra of the free ligands are dominated by intense π–π^* transition bands (mt-qnpy, λ_{max} 196, 202, 220, 278 nm; mt-sexpy, λ_{max} 196, 216, 274, 296 nm), and in the spectra of their transition metal complexes, these bands appear at slightly lower energies but with comparable intensities. In the 400–820-nm region, most of the complexes show absorptions with low to moderate intensities. For example, the Co^{II}(mt-qnpy) complex **2b** shows weak bands at 580 and 475 nm and the energies and

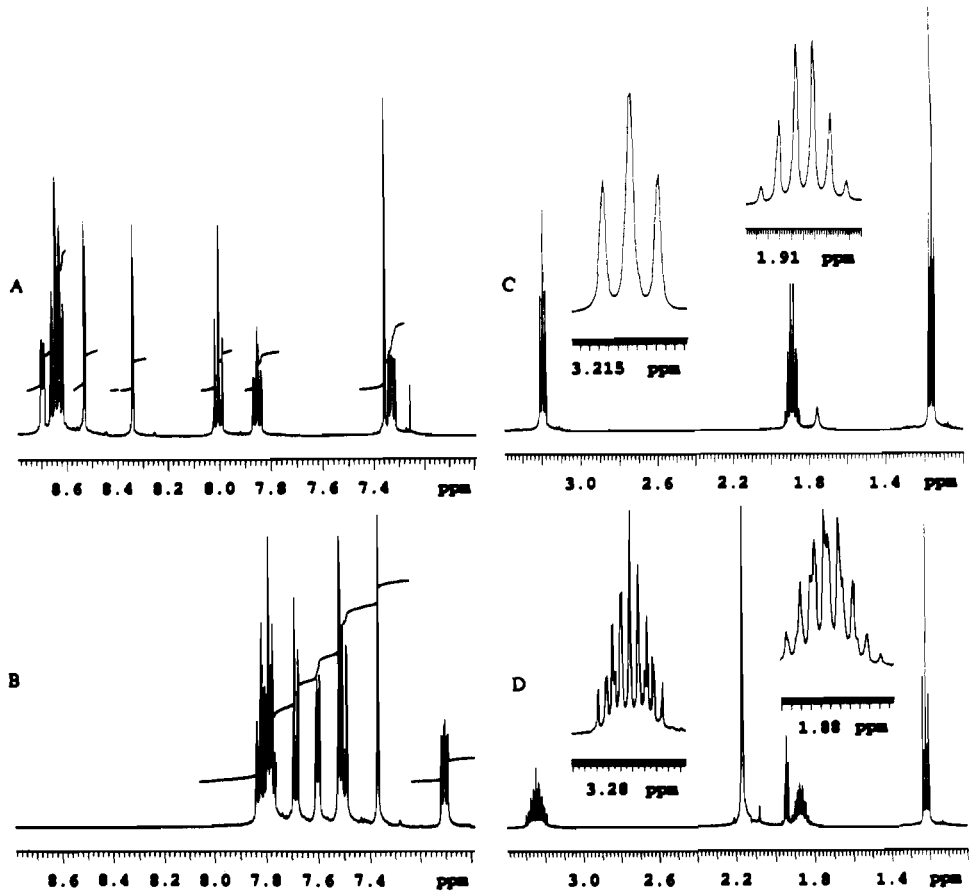

Figure 6. ^{1}H NMR spectra (500 MHz) of the trimetallic Cu(I), double-stranded helical complex **6** derived from the ligand **4b**: (A) ligand **4b** (aromatic region) in $CDCl_3$; (B) complex **6** (aromatic region) in CD_3CN; (C) ligand **4b** (aliphatic region) in $CDCl_3$; (D) complex **6** (aromatic region) in CD_3CN. Insets: Expanded portion of the spectra of the *s*-CH_2–CH_2– groups.

Table III. Chemical Shifts (500 MHz, ppm) and Coupling Constants (Hz) of Protons in the Ligand **4b** and Its Trimetallic, Double-Stranded Helicate **6** in CD_3CN (TMS)

	chem shifts and coupling consts	
proton	ligand **4b**	complex **6**
H_3	8.65, bd, 2H, $J_{4,3}$ = 8.0	7.50, d, 4H, $J_{4,3}$ = 7.7
H_4	7.85, td, 2H, $J_{5,4}$ = $J_{3,4}$ = 8.0, $J_{6,4}$ = 1.2	7.78, td, 4H, $J_{5,4}$ = 7.5, $J_{3,4}$ = 7.7, $J_{6,4}$ = 1.5
H_5	7.32, m, 2H, $J_{4,5}$ = 7.1, $J_{6,5}$ = 4.9	7.10, td, 4H, $J_{4,5}$ = 7.5, $J_{6,5}$ = 5.0, $J_{3,5}$ = 1.2
H_6	8.69, dd, 2H, $J_{5,6}$ = 4.9, $J_{4,6}$ = 1.2	7.60, bd, 4H, $J_{5,6}$ = 5.0
$H_{3'}$	8.34, d, 2H, $J_{5',3'}$ = 1.9	7.52, d, 4H, $J_{5',3'(3',5')}$ = 1.5, ($H_{5'}$)
$H_{5'}$	8.53, d, 2H, $J_{3',5'}$ = 1.9	7.37, d, 4H, $J_{3',5'(5',3')}$ = 1.5, ($H_{3'}$)
$H_{3''}$	8.63, bd, 2H, $J_{4'',3''}$ = 7.4	7.69, d, 4H, $J_{4'',3''}$ = 7.8
$H_{4''}$	8.00, t, 2H, $J_{5'',4''}$ = $J_{3',4'}$ = 7.6	7.82, t, 4H, $J_{5'',4''}$ = $J_{6'',4''}$ = 7.8
$H_{5''}$	8.62, bd, 2H, $J_{4'',5''}$ = 7.4	7.80, d, 4H, $J_{4'',5''}$ = 7.8
$SCH_2CH_2CH_3$	3.20, t, 4H, J_{AM} = 7.4	3.24, m, 8H, ABM_2
$SCH_2CH_2CH_3$	1.91, sext, 4H, J_{AM} = J_{MX} = 7.4	1.87, m, 8H, ABM_2
$SCH_2CH_2CH_3$	1.16, t, 6H, J_{MX} = 7.4	1.22, t, 12H, J_{MX} = 7.3
C_6H_6[a]	7.36, s	

[a] Benzene of crystallization.[8]

intensities of these bands are comparable to those in the spectra of the analogous $[Co^{II}(mt\text{-}terpy)_2][PF_6]_2$ complex and are assigned as MLCT transitions.

The series of complexes derived from mt-sexpy having the general formula $[M(mt\text{-}sexpy)]_2[PF_6]_4$, where M = Co(II), Ni(II), and Cu(II), have UV spectra similar to that of the free ligand as does the Fe(II) complex **5c**. These bands have been assigned as ligand-based π-π^* transitions. In the visible region,

Table IV. Fragment Ions, Relative Abundance, and Assignments for the Ions in the FAB Mass Spectrum of the $[Co^{II}_2(mt\text{-}qnpy)_2OAc][PF_6]_3$ Complex (**2b**)

ion *m/z*	% rel intensity	assgnt
1425	19.3	$[Co^{II}_2(mt\text{-}qnpy)_2OAc(PF_6)_2]^+$
1385	3.9	$[Co^{II}_2(mt\text{-}qnpy)_2(PF_6)_2F]^+$
1366	2.6	$[Co^{II}_2(mt\text{-}qnpy)_2(PF_6)_2]^+$
1299	3.7	$[Co^{II}_2(mt\text{-}qnpy)_2OAc(PF_6)F]^+$
1280	8.6	$[Co^{II}_2(mt\text{-}qnpy)_2OAc(PF_6)]^+$
1240	4.2	$[(Co^{II}_2(mt\text{-}qnpy)_2(PF_6)F]^+$
1221	4.0	$[Co^{II}_2(mt\text{-}qnpy)_2(PF_6)]^+$
597	60	$[Co^{II}_2(mt\text{-}qnpy)]^+$
549	55	$[Co^{II}(mt\text{-}qnpy)F]^+$
538	100	$[Co^{II}(mt\text{-}qnpy)]^+$
524	50	$[Co^{II}(mt\text{-}qnpy)(CH_2)]^+$

the Ni(II) and Co(II) bimetallic complexes **5b,d** exhibited very weak absorptions at 526 and 580 nm, respectively, and the absorption of the Fe(II) complex **5c** was at 508 nm. No visible absorption was observed for the Cu(II) complex **5a**. The trimetallic complex $[Cu^I_3(mt\text{-}sexpy)_2][PF_6]_3$ (**6**) had two absorption bands at 434 and 570 nm, also attributed to MLCT transitions.

X-ray Characterization of Complexes 2c and 5a. Dark-green orthorhombic prisms of complex **2c** with a centrosymmetric space group *Pnna* (No. 52) crystallized from acetonitrile. Figure 1 clearly shows the double-stranded helical geometry of the assembly, which is the result of a major twist occurring between the second and third pyridine rings of the quinquepyridine ligand. This twist divides the ligand strand into a bipy and a terpy segment, each segment bonded to a different Ni(II) ion. As a result the two nickel centers have different chemical environments, Ni(2) with an octahedral N_6 arrangement from the two terpy segments of the two ligand strands and Ni(1) with an octahedral N_4O_2 arrangement from the two bipy segments and a bidentate acetate

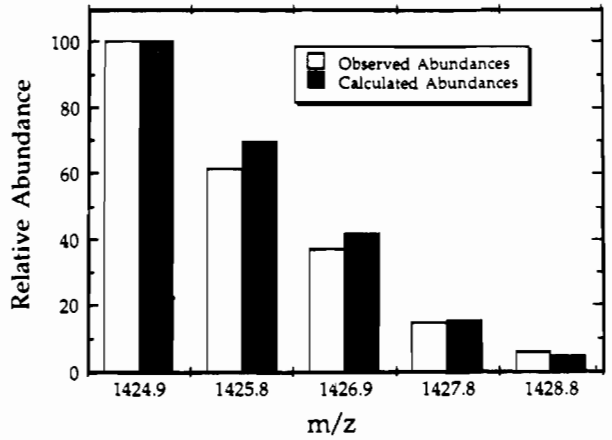

Figure 7. Observed and calculated ion intensities based on isotopic distribution for the ion $[(Co^{II}_2(mt\text{-}qnpy)_2OAc(PF_6)_2]^+$.

Table V. X-ray Structural Parameters of Double-Stranded Bimetallic, Helical Complexes Derived from Ligands **1** and **4**

	complex no.	
	2c, M = Ni(II)	**5a, M = Cu(II)**
R (%)	6.94	6.93
metal–metal dist (Å)	4.42	4.89
pitch height (Å)	8.12	10.42
helical diameter (Å)		
C–C	9.50	9.39
S–S	12.97	12.83
ring interannular angles (deg):	1st strand, 2nd strand	
1, 2; 1A, 2A	15.0; 15.0	13.3; 7.1
2, 3; 2A, 3A	44.0; 44.0	10.0; 12.6
3, 4; 3A, 4A	25.4; 25.4	62.8; 66.9
4, 5; 4A, 5A	3.2; 3.2	16.3; 8.2
5, 6; 5A, 6A		6.0; 14.7
dihedral angles (°) between		
bipy–bipy at M_1	72.9	
terpy–terpy at M_1		83.2
terpy–terpy at M_2	82.2	82.8
av π–π stacking dist between py rings (Å)	3.41	3.44
metal–nitrogen bond lengths (1st strand) (Å)		
N_1–M_1	2.042(6)	2.164(6)
N_2–M_1	2.089(6)	1.965(6)
N_3–M_1		2.294(6)
N_3–M_2	2.220(5)	
N_4–M_2	2.001(6)	2.327(5)
N_5–M_2	2.128(6)	1.965(6)
N_6–M_2		2.143(6)
metal–nitrogen bond lengths (2nd strand) (Å)		
N_{1a}–M_1	2.042(6)	2.172(6)
N_{2a}–M_1	2.089(6)	1.968(6)
N_{3a}–M_1		2.289(5)
N_{3a}–M_2	2.220(5)	
N_{4a}–M_2	2.001(6)	2.291(5)
N_{5a}–M_2	2.128(6)	1.954(6)
N_{6a}–M_2		2.171(6)
metal–oxygen bond length (Å)		
O_{1a}–M_1	2.097(7)	
O_{1aa}–M_1	2.097(7)	

ion. Additional minor twists are present in the bipy and terpy segments, resulting in deviations from coplanarity between the individual pyridine rings. Bond angles associated with the distorted octahedron of Ni(1) are as follows: N(1)–Ni(1)–N(2), 79.0(2)°; N(2)–Ni(1)–N(2A), 110.9(3)°; N(2A)–Ni(1)–N(1A), 79.0(2)°; N(1A)–Ni(1)–O(1A), 84.8(2)°; O(1A)–Ni(1)–O(1AA), 61.9(4)°; O(1AA)–Ni(1)–N(1), 84.8(2)°. The distorted octahedron of Ni(2) has bond angles as follows: N(3)–Ni(2)–N(4), 77.4(2)°; N(4)–Ni(2)–N(5), 77.0(2)°; N(5)–Ni(2)–N(5A), 101.8(3)°; N(5A)–Ni(2)–N(4A), 77.0(2)°; N(4A)–Ni(2)–N(3A), 77.4(2)°; N(3A)–Ni(2)–N(3), 99.7(3)°.

Table V shows various structural parameters of interest for complex **2c**. The Ni atoms are located on the unique 2-fold rotation axis parallel to the *a*-axis of the unit cell. Because of its unique symmetry position, the first strand of the ligand will generate the second strand of the ligand by this unique 2-fold rotation symmetry operation. As a result both strands of the ligand will have identical structural parameters as indicated by ring interannular angles and metal–nitrogen bond lengths shown in Table V. With the two carbon atoms of the acetate group also being located on this unique 2-fold axis, the methyl hydrogens of the acetate group are inherently present in two conformations with 50% site occupancy for each conformation. Coplanar stacking interactions are present between parallel pyridine rings in the two strands, with the average π–π stacking distance between approximately parallel strands of the ligand being 3.41 Å. The nonbonded distance of Ni(1)–Ni(2) is 4.42 Å.

The complex **5a** [space group $P2_1/c$ (No. 14)] crystallized as green, monoclinic prisms from an acetonitrile solution with slow diffusion of diethyl ether. Figure 2 shows the double-stranded helical geometry of the complex, which is the result of a major twist occurring between the third and fourth pyridine rings in the sexipyridine chain. This twist divides the ligand strand into two terpy subunits, each bonded to a different Cu(II) ion. As a result, both Cu(II) centers have the same octahedral N_6 environment from the two terpy segments of each strand. Additional minor twists were present in the terpy segments resulting in small deviations from coplanarity between the individual rings. This deviation is not, however, as pronounced as in complex **2c** above. Table V presents values for these parameters. Unlike in the quinquepyridine complex **2c** described above, the 2-fold rotation axis which passes through the metal–metal axis is absent in **5a**. Thus, the two ligand strands have different structural parameters as indicated in ring interannular angles and metal–nitrogen bond lengths (Table V). The distorted octahedron of Cu(1) has the following bond angles: N(1)–Cu(1)–N(2), 77.6(2)°; N(2)–Cu(1)–N(3), 76.9(2)°; N(3)–Cu(1)–N(3A), 96.5(2)°; N(3A)–Cu(1)–N(2A), 76.2(2)°; N(2A)–Cu(1)–N(1A), 78.1(2)°; N(1A)–Cu(1)–N(1), 105.4(2)°. The distorted octahedron of Cu(2) has the following bond angles: N(4)–Cu(2)–N(5), 76.0(2)°; N(5)–Cu(2)–N(6), 78.8(2)°; N(6)–Cu(2)–N(6A), 106.4(2)°; N(6A)–Cu(2)–N(5A), 77.9(2)°; N(5A)–Cu(2)–N(4A), 75.5(2)°; N(4A)–Cu(2)–N(4), 96.4(2)°.

Once again coplanar stacking interactions are present between parallel rings of the two strands. The average π–π stacking distance between approximately parallel strands of the ligand is 3.44 Å, and the nonbonded Cu(1)–Cu(2) distance is 4.89 Å.

Electrochemical Measurements. In general, most of the complexes studied exhibited rich electrochemical behavior. In a number of cases, more than one metal-based oxidation (and in some cases metal-based reductions as well) were observed. When the metal centers have the same coordination environment, this redox behavior is an indication of significant metal–metal interaction. A compilation of the formal potentials for the bimetallic complexes with mt-qnpy and mt- or pt-sexpy ligands and related complexes is given in Table VI. For comparison purposes, electrochemical data on monometallic octahedral complexes of the type $[M(mt\text{-}terpy)_2][PF_6]_2$ (where mt = methylthio) is included. In the following discussion the complexes of a particular metal are considered as a group.

Cobalt Complexes. Figure 8 shows cyclic voltammograms for $[Co^{II}_2(mt\text{-}qnpy)_2OAc][PF_6]_3$ (**2b**) and $[Co^{II}(mt\text{-}sexpy)]_2(PF_6)_4$ (**5d**) in acetonitrile. In the potential region from 0.0 to +2.0 V, complex **5d** had two reversible, one-electron oxidations at +0.93 and +1.32 V, respectively, which correspond to the Co(II/III) oxidation of each metal center (Figure 8A). It is clear that the metal centers in this complex oxidize at very different potentials with a $\Delta E°'$ value of 390 mV. The difference in metal-based oxidation potentials in symmetric homobimetallic complexes has previously been used as a measure of the degree of metal–metal communication, and this large value of $\Delta E°'$ observed in the

Table VI. Formal Potentials vs SSCE for the Ligands **1** and **4** and Their Complexes at a Platinum Electrode in a 0.1 M solution of TBAP[a]

ligand/complex no.	solvent	$E^{\circ\prime}$ (V) [ΔE_p (mV)]
1a	CH_3CN	−1.88 [irrev]
$\{[Co^{II}(mt\text{-}qnpy)]_2CH_3CO_2\}[PF_6]_3$ (**2b**)	CH_3CN	+0.87 [80], +1.09 [80], −0.66 [70], −1.02 [100], −1.28 [70], −1.70 [70], −1.94 [80], −2.13 [100]
$\{[Ni^{II}(mt\text{-}qnpy)]_2CH_3CO_2\}[PF_6]_3$ (**2c**)	DMF	−0.82 [70], −1.26 [50], −1.45 [60], −1.97 (2e⁻) [50]
$\{[Zn^{II}(mt\text{-}qpny)]_2CH_3CO_2\}[PF_6]_3$ (**2d**)	CH_2Cl_2	−1.80 [80], −1.88 [60]
$[Pd^{II}(mt\text{-}qnpy)]_2[PF_6]_4$ (**2e**)	CH_3NO_2	−1.65 [irrev]
$[Cu^{II}(mt\text{-}sexpy)]_2[PF_6]_4$ (**5a**)	CH_3CN	+0.45 [irrev], +0.02 [90], −1.38 [60], −1.61 [60], −1.78 [130], −1.91 [130]
	DMF	+0.49 [irrev], +0.06 [50], −1.30 [60], −1.50 [50], −1.70 [50], −1.87 [60], −2.15 [60]
	DMSO	+0.38 [irrev], +0.06 [irrev], −1.02 [60], −1.32 [60], −1.52 [60], −1.67 [110]
$[Ni^{II}(mt\text{-}sexpy)]_2[PF_6]_4$ (**5b**)	CH_3CN	−1.00 (2e⁻) [60], −1.32 [80], −1.57 [90], −1.90 [irrev]
	DMF	−0.92 [70], −1.13 [60], −1.35 [60], −1.91 [irrev]
$[Fe^{II}(pt\text{-}sexpy)]_2[ClO_4]_4$ (**5c**)	CH_3CN	+1.34 [60], +1.22 [60], −0.80 [60], −0.97 [60], −1.12 [60], −1.42 [ads], −1.33 [strip]
$[Co^{II}(mt\text{-}sexpy)]_2[PF_6]_4$ (**5d**)	DMF	−0.52 [50], −0.67 [60], −1.45 [60], −1.60 [60], −1.82 [80], −1.98 [60]
	CH_3CN	+0.93 [60], +1.32 [60], −0.63 [60], −0.76 [50], −1.55 [60], −1.73 [70], −1.93 [60], −2.07 [60]
$[Cu^{I}_3(pt\text{-}sexpy)_2][PF_6]_3$ (**6**)	CH_3CN	+0.42 [irrev], +0.06 [irrev], −1.41 [60], −1.63 [60], −1.84 [80], −1.98 [100]
$[Co^{II}(mt\text{-}terpy)_2][PF_6]_2$	CH_3CN	+0.21 [70], −0.84 [80], −1.65 [70]
$[Ni^{II}(mt\text{-}terpy)_2][PF_6]_2$	CH_3CN	+1.70 [80]
	DMSO	−1.18 [100], −1.38 [120]
$[Fe^{II}(mt\text{-}terpy)_2][PF_6]_2$	CH_3CN	+1.03 [70], −1.29 [70], −1.38 [70]

[a] Except when indicated, the processes appeared to be one-electron transfers.

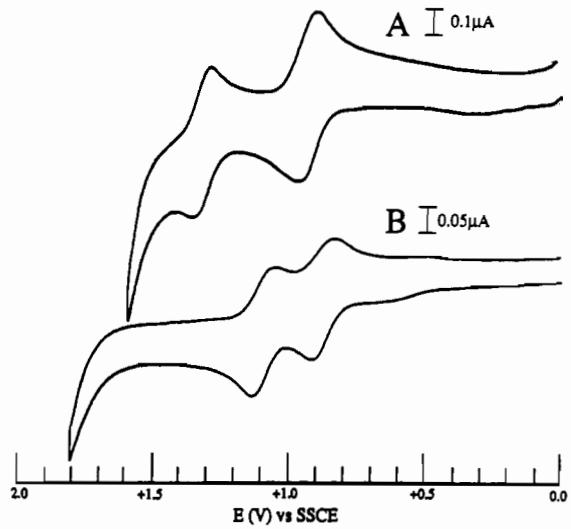

Figure 8. Cyclic voltammograms of (A) $[Co^{II}(mt\text{-}sexpy)]_2[PF_6]_4$ (**5d**) and (B) $[Co^{II}_2(mt\text{-}qnpy)_2OAc][PF_6]_3$ (**2b**) in 0.1 M TBAP/CH_3CN.

present case is indicative of a high degree of metal–metal interaction.[2] As a result, the complex does not behave as merely two independent $[Co^{II}(mt\text{-}terpy)_2]^{2+}$ units but rather as a bimetallic species with appreciable electronic communication occurring between the metal centers. Both Co(II/III) oxidation potentials were significantly more positive than that for the complex $[Co^{II}(mt\text{-}terpy)_2][PF_6]_2$, which oxidized at +0.21 V.

The helicate $[Co^{II}_2(mt\text{-}qnpy)_2OAc][PF_6]_3$ (**2b**) having a different chemical environment around each Co center (N_6 and N_4O_2) is not symmetric and presents a more complicated case. The electrochemical response of this complex in acetonitrile solution, when scanning in the negative region between 0.0 and −2.0 V (*vide infra*), suggests that the acetate ligand is probably displaced by one or two solvent molecules. The formal potentials for the two Co(II/III) couples in **2b** were observed at +1.09 and +0.87 V (Figure 8B). The inherent asymmetric environment around the two metal centers precludes an analysis of the difference in formal potentials in terms of metal–metal interaction since such a difference could well be due to the difference in coordination environments.

At negative potentials, both complexes underwent numerous reversible reductions. The complex **5d** had six reversible one-electron reductions in the potential region from 0.0 to −2.0 V

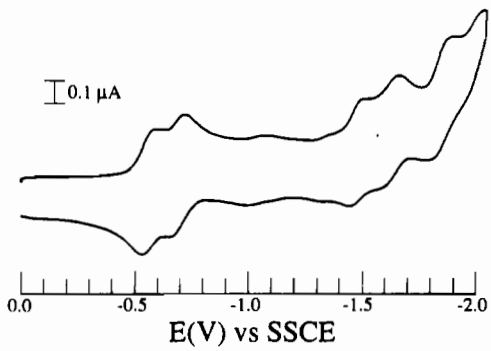

Figure 9. Cyclic voltammogram of $Co^{II}(mt\text{-}sexpy)]_2[PF_6]_4$ (**5d**) in 0.1 M TBAP/DMF.

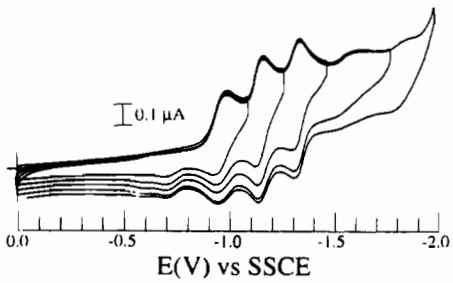

Figure 10. Cyclic voltammogram of $[Co^{II}_2(mt\text{-}qnpy)_2OAc][PF_6]_3$ (**2b**) in 0.1 M TBAP/DMF.

(Figure 9). By analogy to other Co complexes, the first two waves at −0.63 and −0.76 V were assigned to Co(II/I) processes at each of the metal centers. These reductions are positive relative to that for $[Co^{II}(mt\text{-}terpy)_2][PF_6]_2$, whose Co(II/I) reduction is at −0.84 V. This result is consistent with the shifts observed in the oxidation potentials. The difference in formal potentials between the two metal-based reductions, 130 mV, is considerably smaller than that seen in the oxidations. There are, in addition, four reversible one-electron redox processes at −1.55, −1.73, −1.93, and −2.07 V due to ligand-localized reductions.

The electrochemical response of the complex **2b** was found to depend significantly on the coordinating ability of the solvent. In relatively weak coordinating solvents, such as DMF, this complex showed five reversible, one-electron reductions in the negative potential region at −0.90, −1.13, −1.31, −1.56, and −1.79 V (Figure 10). Similar behavior was observed in DMSO with reductions at very similar potentials with the exception of the first reduction

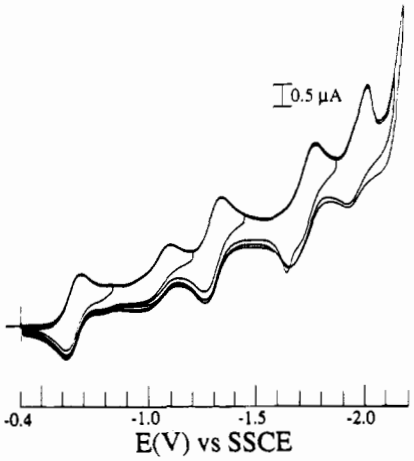

Figure 11. Cyclic voltammogram of $[Co^{II}_2(mt\text{-}qnpy)_2OAc][PF_6]_3$ (**2b**) in 0.1 M TBAP/CH_3CN.

which is shifted slightly to –0.95 V. The first two waves are attributed to the Co(II/I) reduction of the individual cobalt centers by comparing these values to those obtained for the complex **5d**. Such a difference in metal-reduction potentials is expected since the increase in electron density on the Co bound to the acetate (N_4O_2) group will shift its reduction negative of that for the Co bonded to six pyridine (N_6) groups. The complex had three additional reductions at –1.31, –1.56, and –1.79 V which are again ascribed to ligand-based processes.

In acetonitrile solvent the first two reductions for complex **2b** were shifted to less negative potentials, to –0.66 and –0.97 V (Figure 11). This is likely due to substitution of the acetate ligand by one or more acetonitrile ligands. The first reduction at –0.66 V may then be assigned to the Co center bound to four pyridines and one or more acetonitrile ligands, whereas the process at –0.97 V is probably due to the Co center bound to six pyridines. Previous electrochemical studies with $[Co^{II}(terpy)_2][PF_6]_2$ have indicated[13] that bound acetonitrile is a significantly better π acceptor than pyridine, and this is consistent with the observed shifts. It should be mentioned that the potentials for the metal-based oxidations were also shifted in a manner consistent with the substitution of the acetate ligand by acetonitrile. The complex had three additional reductions at –1.28, –1.70, and –1.94 V assigned to ligand-based processes.

The electrochemical behavior of a related cobalt complex derived from a nonfunctionalized quinquepyridine ligand has been reported,[10a] and in that study three small and poorly defined oxidations as well as numerous reductions of widely varying intensities were observed. Furthermore the authors report that all the voltammetric features were scan rate dependent. In contrast to that study, we have described above two well-resolved one-electron metal-based oxidations and reductions corresponding to Co(II/III) and Co(II/I) processes, respectively, and these results were not unanticipated. We have also observed a series of well-resolved ligand-based reductions. In addition, the processes were virtually independent of sweep rate (except for a slight increase in the peak separation due to ohmic drop in solution). We cannot reconcile these differences which we believe are likely due to impurities or to a mixture of monometallic, bimetallic species, etc. in the complex or impurities in the solvent/supporting electrolyte employed in their study.

Nickel Complexes. The complexes $[Ni^{II}_2(mt\text{-}qnpy)_2OAc][PF_6]_3$ (**2c**) and $[Ni^{II}(mt\text{-}sexpy)]_2[PF_6]_4$ (**5b**) showed no voltammetric response in the potential region from 0.0 to +1.8 V in acetonitrile. As previously mentioned, the Co complexes of mt-qnpy and of mt-sexpy oxidize at much more positive potentials (by about 600 mV) than does $[Co^{II}(mt\text{-}terpy)_2][PF_6]_2$. Since $[Ni^{II}(mt\text{-}terpy)_2][PF_6]_2$ itself oxidizes at +1.70 V, then, reasoning by analogy, it is anticipated that the mt-qnpy Ni(II) complex **2c** and mt-sexpy Ni(II) complex **5b** would oxidize at considerably more positive potentials and thus outside the solvent potential window.

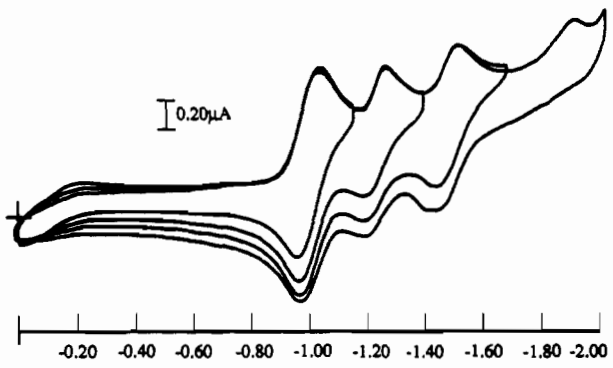

Figure 12. Cyclic voltammogram of $[Ni^{II}(mt\text{-}sexpy)]_2[PF_6]_4$ (**5b**) in 0.1 M TBAP/CH_3CN.

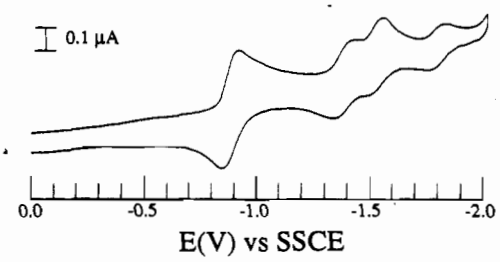

Figure 13. Cyclic voltammogram of $[Ni^{II}(mt\text{-}qnpy)_2OAc][PF_6]_3$ (**2c**) in 0.1 M TBAP/CH_3CN.

In the negative region from 0.0 to –2.0 V, $[Ni^{II}(mt\text{-}sexpy)]_2[PF_6]_4$ (**5b**) underwent four reduction processes (Figure 12). The first at –1.00 V was a reversible two-electron wave consistent with the simultaneous Ni(II/I) reduction of both nickel centers. This wave is 330 mV more positive than the corresponding reduction in $[Ni^{II}(mt\text{-}terpy)_2][PF_6]_2$. This result is analogous to that described above for the cobalt complexes. There are, in addition, three one-electron ligand-based reductions at –1.32, –1.57, and –1.90 V which are independent of solvent. These waves have been assigned as ligand-centered reductions on the basis of the analogous copper complex which undergoes ligand reductions at comparable potentials.

The complex $[Ni^{II}_2(mt\text{-}qnpy)_2OAc][PF_6]_3$ (**2c**) exhibited a reversible two-electron wave at –0.87 V, which corresponds to the simultaneous reduction of both Ni centers (Figure 13). Controlled-potential coulometry after this wave, at –1.20 V, yielded an n value of 2.16 electrons. It is interesting to note that although the chemical environment around each nickel center in this case is quite different, both metal centers appear to undergo reduction at the same potential. Previous studies have indicated that the potential for the metal-based reduction in $[Ni^{II}(terpy)_2]^{2+}$ is about 100 mV more negative than the corresponding process in $[Ni^{II}(bipy)_3]^{2+}$. It would be anticipated, therefore, that the nickel center bound to two terpyridine-like groups in $[Ni^{II}_2(mt\text{-}qnpy)_2OAc][PF_6]_3$ (**2c**) would reduce at more negative potentials than the nickel bound to bipyridine-like groups. In this case, however, the latter is also bound to an electron-donating acetate group, which would also shift its reduction potential in a negative fashion. These combined effects appear to shift the reduction of the nickel centers to the same potential. On the basis of the analogous copper complex[5a] (*vide infra*), we also assign the three waves at –1.32 V, –1.57, and –1.90 V as corresponding to ligand-based reductions.

Iron Complexes. The complex $[Fe^{II}_2(mt\text{-}qnpy)_2OAc][PF_6]_3$ (**2a**) had very low solubility in most solvents except DMF. This complex showed no voltammetric response in the region between 0.00 and +1.60 V (solvent limit). In the negative potential region,

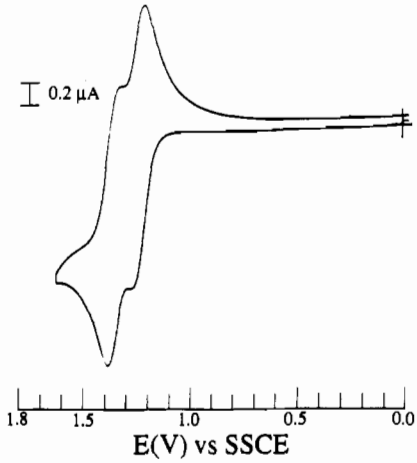

Figure 14. Cyclic voltammogram of $[Fe^{II}(pt\text{-}sexpy)]_2[ClO_4]_4$ (**5c**) in 0.1 M TBAP/CH_3CN.

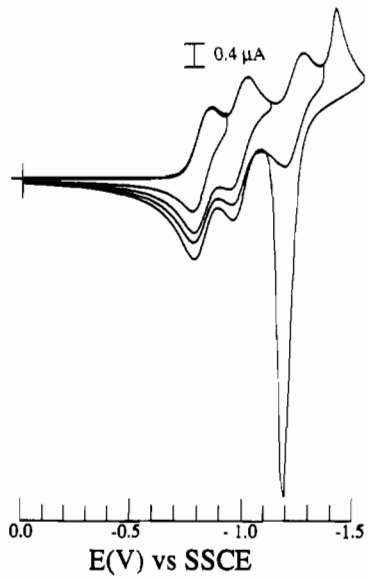

Figure 15. Cyclic voltammogram of $[Fe^{II}(pt\text{-}sexpy)]_2[ClO_4]_4$ (**5c**) in 0.1 M TBAP/CH_3CN.

there was an ill-defined, irreversible wave at −1.23 V and an additional quasi-reversible wave at −1.86 V.

The complex $[Fe^{II}(mt\text{-}sexpy)]_2[ClO_4]_4$ (**5c**) exhibited two reversible, metal-centered, one-electron redox processes at +1.34 and +1.22 V in acetonitrile solution corresponding to Fe(II)/Fe(III) oxidations (Figure 14). These oxidations have a smaller $\Delta E^{\circ\prime}$ (120 mV) than that shown by the analogous cobalt complex **5d**. However, the difference in oxidation potentials in this case also indicates a significant degree of metal–metal interaction. In the negative potential region, there are three one-electron reversible processes at −0.80, −0.97, and −1.12 V, as well as a wave with a peak potential value of −1.42 V which leads to adsorption on the electrode surface (Figure 15). This is likely due to the fact that at potentials beyond −1.42 V the complex is neutral and thus prone to adsorb.

Palladium and Zinc Complexes. The complexes $[Pd^{II}(mt\text{-}qnpy)]_2[PF_6]_4$ (**2e**) and $[Zn^{II}_2(mt\text{-}qnpy)_2OAc][PF_6]_3$ (**2d**) showed no voltammetric response upon scanning in the positive direction to +2.00 and +1.60 V, respectively. Upon scanning in the negative direction in acetonitrile solution, the Pd complex showed one irreversible wave at −1.65 V, which is likely ligand based. The voltammetric response for the Zn complex exhibited some solvent dependence implying the displacement of the acetate groups by solvent molecules. In acetonitrile solution (Figure 16) the complex underwent four one-electron ligand-based reductions at −1.06, −1.25, −1.47, and −2.02 V whereas in DMSO solution they were

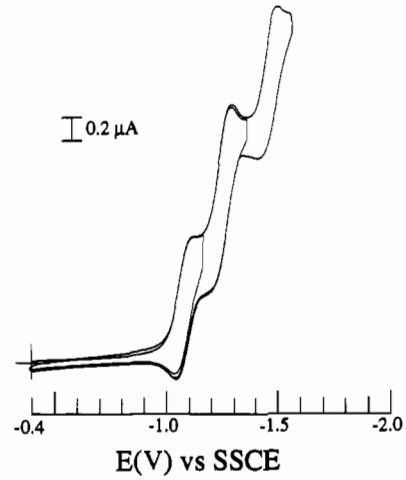

Figure 16. Cyclic voltammogram of $[Zn^{II}_2(mt\text{-}qnpy)_2OAc][PF_6]_3$ (**2d**) in 0.1 M TBAP/CH_3CN.

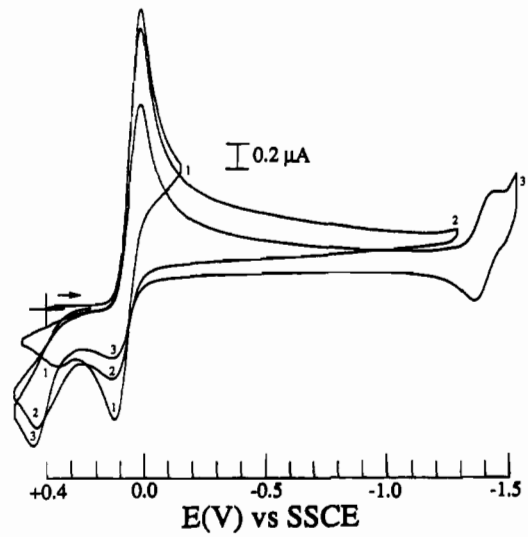

Figure 17. Cyclic voltammogram of $[Cu^{II}(mt\text{-}sexpy)]_2[PF_6]_4$ (**5a**) in 0.1 M Bu_4NPF_6/CH_3CN.

observed at −1.10, −1.36, −1.86, and −2.05 V. The shift in the ligand reductions observed in acetonitrile is in agreement with the displacement of the acetate ligand with solvent molecules.

Copper Complexes. The dimetallic complex $[Cu^{II}(mt\text{-}sexpy)]_2[PF_6]_4$ (**5a**) showed very interesting electrochemical activity which was not observed for the complexes of the other transition metals studied. Figure 17 shows the cyclic voltammogram for the complex **5a** in acetonitrile in the potential region +0.40 and −1.50 V. The voltammetric scan was started at +0.40 V since at this potential the complex retains a Cu(II)/Cu(II) state in solution. As the potential was scanned negatively, a two-electron wave was observed at +0.02 V, corresponding to the simultaneous one-electron reduction of each Cu center. Upon scan reversal at −0.10 V (Figure 17, trace 1), an anodic wave was observed at −0.11 V corresponding to the two-electron re-oxidation of the Cu(I)/Cu(I) complex to the Cu(II)/Cu(II) species. A smaller additional peak was observed at +0.45 V. During the second and third scans, when the scan was reversed at more negative potentials (Figure 17, traces 2 and 3), the peak at +0.45 V was observed to increase while the return peak at −0.11 V decreased. From their respective cyclic voltammograms it was possible to determine that the new peak observed at +0.45 V corresponded to the oxidation of a trimetallic species $[Cu^{I}_3(mt\text{-}sexpy)_2][PF_6]_3$ (**6**) generated as a product of the reduction of the original dimetallic complex $[Cu^{II}(mt\text{-}sexpy)]_2[PF_6]_4$ (**5a**).

The trimetallic complex $[Cu^{I}_3(mt\text{-}sexpy)_2][PF_6]_3$ (**6**) was synthesized by an alternative method and characterized. Its

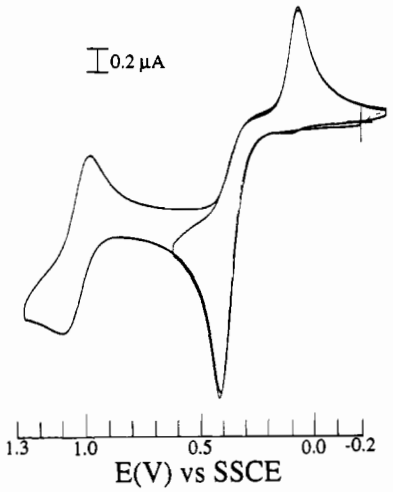

Figure 18. Cyclic voltammogram of $[Cu^{I}_3(pt\text{-}sexpy)_2][PF_6]_3$ (**6**) in 0.1 M Bu_4NPF_6/CH_3CN.

Scheme III. Redox Processes Involved for Complex **5a**

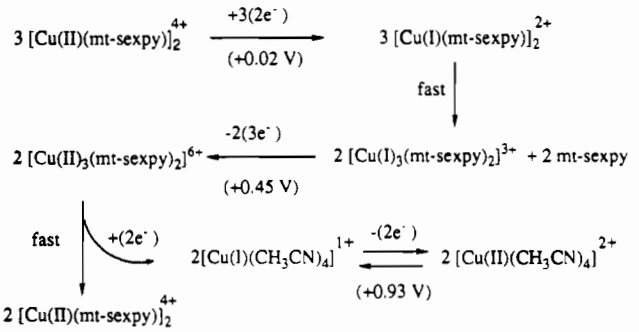

voltammetric response in the region between +1.30 and –0.20 V is shown in Figure 18, the voltammetric scan being started at –0.20 V since at this potential the complex retained its Cu(I)/Cu(I)/Cu(I) trimetallic structure in solution. The two-electron wave observed at +0.42 V corresponds to the simultaneous oxidation of two copper centers with the concomitant ejection of a Cu(I) ion. This is the same process observed in the cyclic voltammogram of $[Cu^{II}(mt\text{-}sexpy)]_2[PF_6]_4$ (**5a**) as a new peak at +0.45 V. In acetonitrile, the oxidation of the ejected Cu(I) ion was observed as a quasi-reversible wave at +0.93 V. This potential is identical to that obtained for a sample of $[Cu^{I}(CH_3CN)_4]^+$ in acetonitrile solution. Upon reversal at +1.0 V, there is a small wave at +0.34 V which is associated with the process observed at +0.42 V. But more importantly, a two-electron wave corresponding to the reduction of a Cu(II)/Cu(II) dimetallic species was observed at +0.06 V. This dimetallic species was formed as a product of the oxidation of the trimetallic species. These processes are described in Scheme III. Additional studies for elucidation of the kinetics of these transformations employing fast scan cyclic voltammetry at microelectrodes and chronoamperometry along with computer simulations are currently ongoing and will be reported elsewhere.[14]

Both the dimetallic and trimetallic systems exhibit four reversible reductions in the negative potential region at about the same potentials. For the dimetallic system, those reductions were observed at formal potentials of –1.38, –1.61, –1.78, and –1.91 V (Figure 19), which, by analogy to the previously described complexes, are assigned to ligand-based processes. As shown in Figure 19, the complex appears to adsorb after the third reduction as shown by the stripping peak at –1.80 V.

The transformation of the dimetallic to the trimetallic species and vice versa was studied further by spectroelectrochemistry, which allows for the investigation of structural changes in the complexes by observing changes in their visible spectra as a function of applied potential. Figure 20 shows the visible spectra

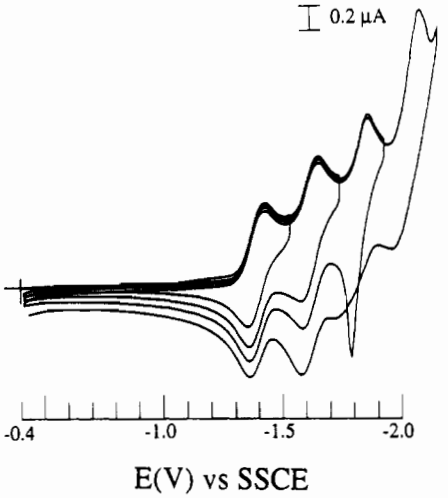

Figure 19. Cyclic voltammogram of $[Cu^{II}(mt\text{-}sexpy)]_2[PF_6]_4$ (**5a**) in 0.1 M Bu_NPF_6/CH_3CN.

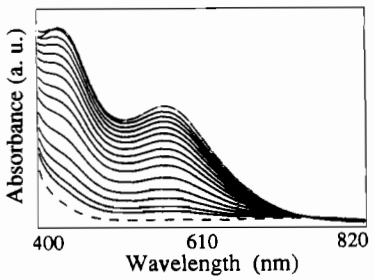

Figure 20. Visible spectra of (- - -) $[Cu^{II}(mt\text{-}sexpy)]_2[PF_6]_4$ (**5a**) and (—) $[Cu^{II}(mt\text{-}sexpy)]_2[PF_6]_4$ (**5a**) at an applied potential of –0.20 V and (– · –) $[Cu^{I}_3(pt\text{-}sexpy)_2][PF_6]_3$ (**6**).

of a solution of $[Cu^{II}(mt\text{-}sexpy)]_2[PF_6]_4$ (**5a**) in 0.1 M TBAP/CH_3CN taken every 3 min as the potential of the Pt gauze working electrode was held at –0.40 V. The dashed line (lower-most trace) represents the spectrum of $[Cu^{II}(mt\text{-}sexpy)]_2[PF_6]_4$ (**5a**) taken before electrolysis, which shows very little absorption in the visible region. As the solution was electrolyzed at –0.40 V, the visible spectrum showed the appearance of two absorption bands at λ_{max} values of 434 and 570 nm. The shape and energy of these absorption bands are characteristic of the trimetallic complex $[Cu^{I}_3(mt\text{-}sexpy)_2][PF_6]_3$ (**6**). The final spectrum taken after 45 min of electrolysis was found to be identical to that of a chemically synthesized sample of $[Cu^{I}_3(mt\text{-}sexpy)_2][PF_6]_3$ (**6**) in 0.1 M TBAP/CH_3CN, the spectrum of which is also shown in Figure 20 for comparison purposes (topmost trace). When the reddish-brown solution of electrochemically generated $[Cu^{I}_3(mt\text{-}sexpy)_2][PF_6]_3$ (**6**) was electrolyzed at +0.60 V for 1 h, the spectrum of the dimetallic Cu(II)/Cu(II) complex was recovered, albeit not to completion, since the initial process involved some ligand loss (see Scheme III).

A similar spectroelectrochemical experiment was carried out with $[Cu^{I}_3(mt\text{-}sexpy)_2][PF_6]_3$ (**6**) in solution, and the spectra obtained are shown in Figure 21. In this case, the electrode was held at a potential of +0.60 V. The dashed line (topmost spectrum) represents the spectrum of $[Cu^{I}_3(mt\text{-}sexpy)_2][PF_6]_3$ (**6**) obtained before electrolysis, while the solid lines represent the spectra taken every 2 min at an applied potential of +0.60 V. The spectrum obtained after 1 h of electrolysis at +0.60 V was very close to that of the Cu(II)/Cu(II) dimer. There is some residual absorbance which is attributed to the presence of some starting material.

Conclusions

The use of soluble and functionalized quinquepyridine and sexipyridine ligands at ambient temperature enables us to utilize

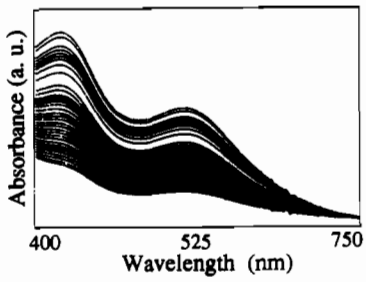

Figure 21. Visible spectra of (- · -) $[Cu^{I}_3(pt\text{-}sexpy)]_2[PF_6]_3$ (**6**) and (—) $[Cu^{I}_3(pt\text{-}sexpy)_2][PF_6]_3$ (**6**) at an applied potential of -0.60 V.

the high specificity and efficiency of self-assembly processes and provides an entry into a broad family of transition metal complexes. These complexes possess unusual and interesting structural and reactivity behaviors.

The *S-n*-propyl substituents located in an external 4-pyridyl position is ideally situated for use as an ^1H NMR probe in diamagnetic complexes, and their NMR patterns have enabled us to determine conveniently the solution stability of these complexes in a variety of polar solvents. These NMR data have also provided direct evidence for the helical chirality of the complexes and emphasize the importance of substituents located on the outer periphery of the helix.

The electrochemical behavior exhibited by the Co(II) and Fe(II) complexes (differences in formal potential of metal centers in identical coordination environments) of functionalized sexipyridine provides strong indication of metal–metal interaction. In contrast, with the functionalized quinquepyridine–Co(II) complex, in spite of its rich electrochemistry, no definitive conclusions concerning metal–metal interaction can be drawn from electrochemical measurements alone since the two cations have different chemical environments.

Tetrahedral and octahedral recognition by the functionalized sexipyridine ligand by Cu(I) and Cu(II), respectively, and the highly efficient interconversions of the resulting complexes, which have been verified spectroelectrochemically, are the result of the electronic configuration of the metal cation. Applications of these interconversions based on the ejection of one Cu(I) in oxidation processes and the converse, the incorporation of Cu(I) in reduction processes, are intriguing. We are currently studying these interconversions as an approach to the synthesis of heteropolymetallic complexes.

Our systematic study of the double-stranded polymetallic helicates derived from functionalized terpyridine, quaterpyridine, quinquepyridine, and sexipyridine now provide guidelines for future directions in this area. In these oligopyridines, the complexity of these interconversions with the increase in the number of ligating units increases significantly. For example a similarly functionalized septipyridine, an odd-numbered ligand, follows the same trend as has been observed with functionalized terpyridine[15] and quinquepyridine,[5a] and we have currently identified four copper helicates which will be described in a future publication. We are also observing with a functionalized octipyridine, an even-numbered ligand, characteristics similar to those shown by quaterpyridine[5a] and sexipyridine. Thus, there appears to be odd–even patterns of behavior in these polymetallic helicates, and these are areas that we are currently pursuing.

Acknowledgment. We thank Dr. R. Kullnig for his interest and encouragement during the X-ray structural determinations, and the NSF (Grant CHE-9105906) and USPHS (Grant S10RR06245) for funds for the purchase of the 500-MHz NMR spectrometer. Mass spectra were carried out at the University of Illinois by Dr. R. Milberg and S. Mullen to whom we express our thanks. Partial support of this work by the American Cyanamid Co. (K.P.) and the Materials Science Center at Cornell University (C.A. and H.D.A.) is gratefully acknowledged.

Supplementary Material Available: Tables providing full details of the X-ray structural determinations including crystal data, atomic coordinates and isotropic thermal parameters, bond lengths, bond angles, anisotropic thermal parameters, and H-atom coordinates and isotropic thermal parameters for complexes **2c** and **5a** (23 pages). Ordering information is given on any current masthead page.